bioRxiv preprint doi: https://doi.org/10.1101/2022.01.19.477024; this version posted January 21, 2022. The copyright holder for this preprint (which was not certified by peer review) is the author/funder, who has granted bioRxiv a license to display the preprint in perpetuity. It is made available under aCC-BY-NC-ND 4.0 International license.

Environment constrains fitness advantages of division of labor in microbial consortia engineered for metabolite push or pull interactions

Ashley E. Beck[1,4], Kathryn Pintar[1,a], Diana Schepens[2,b], Ashley Schrammeck[1,c], Timothy Johnson[1,d], Alissa Bleem[1,e], Martina Du[1], William R. Harcombe[3], Hans C. Bernstein[5], Jeffrey J. Heys[1], Tomas Gedeon[2], Ross P. Carlson[1]

[1.] *Department of Chemical and Biological Engineering, Montana State University, Bozeman, MT, USA*

[2.] *Department of Mathematics and Statistics, Montana State University, Bozeman, MT, USA*

[3.] *Department of Ecology, Evolution, and Behavior, University of Minnesota, St. Paul, MN, USA*

[4.] *Department of Biological and Environmental Sciences, Carroll College, Helena, MT, USA*

[5] *Norwegian College of Fisheries Sciences & The Arctic Centre for Sustainable Energy, UiT - The Arctic University of Norway, Tromsø, Norway*

[a.] *current address: Seeq! Inc., St. Paul, MN, USA*

[b.] *current address: Whitworth College, Spokane, WA, USA*

[c.] *current address: Glaxo Smith Kline Inc., Hamilton, MT, USA*

[d.] *current address: Bechtel National Inc, Richland, WA, USA*

[e] *current address: Renewable Resources and Enabling Sciences Center, National Renewable Energy Laboratory, Golden, CO 80401, USA*

bioRxiv preprint doi: https://doi.org/10.1101/2022.01.19.477024; this version posted January 21, 2022. The copyright holder for this preprint (which was not certified by peer review) is the author/funder, who has granted bioRxiv a license to display the preprint in perpetuity. It is made available under aCC-BY-NC-ND 4.0 International license.

ABSTRACT

Fitness benefits from division of labor in microbial consortia are well documented, but the dependency of the benefits on environmental context is poorly understood. Two synthetic *Escherichia coli* consortia were built to test the relationships between exchanged organic acid, local environment, and opportunity costs of different metabolic strategies. Opportunity costs quantify benefits not realized due to selecting one phenotype over another. The consortia catabolized glucose and exchanged either acetic or lactic acid to create producer-consumer food webs. The organic acids had different inhibitory properties and different opportunity costs associated with their positions in central metabolism. The exchanged metabolites modulated different consortial dynamics. The acetic acid-exchanging (AAE) consortium had a 'push' interaction motif where acetic acid was secreted faster by the producer than the consumer imported it, while the lactic acid-exchanging (LAE) consortium had a 'pull' interaction motif where the consumer imported lactic acid at a comparable rate to its production. The LAE consortium outperformed wild type (WT) batch cultures under the environmental context of weakly buffered conditions, achieving a 55% increase in biomass titer, a 51% increase in biomass per proton yield, an 86% increase in substrate conversion, and the complete elimination of byproduct accumulation all relative to the WT. However, the LAE consortium had the tradeoff of a 42% lower specific growth rate. The AAE consortium did not outperform the WT in any considered fitness metric. Fitness advantages of the LAE consortium were sensitive to environment; increasing the medium buffering capacity negated the fitness advantages compared to WT.

IMPORTANCE

Most naturally occurring microorganisms persist in consortia where metabolic interactions are common and often essential to ecosystem function. This study uses synthetic ecology to test how different cellular interaction motifs influence fitness properties of consortia. Environmental

bioRxiv preprint doi: https://doi.org/10.1101/2022.01.19.477024; this version posted January 21, 2022. The copyright holder for this preprint (which was not certified by peer review) is the author/funder, who has granted bioRxiv a license to display the preprint in perpetuity. It is made available under aCC-BY-NC-ND 4.0 International license.

context ultimately controlled the division of labor fitness as shifts from weakly buffered to highly buffered conditions negated the benefits of the strategy. Understanding the limits of division of labor advances our understanding of natural community functioning which is central to nutrient cycling and provides design rules for assembling consortia used in applied bioprocessing.

bioRxiv preprint doi: https://doi.org/10.1101/2022.01.19.477024; this version posted January 21, 2022. The copyright holder for this preprint (which was not certified by peer review) is the author/funder, who has granted bioRxiv a license to display the preprint in perpetuity. It is made available under aCC-BY-NC-ND 4.0 International license.

INTRODUCTION

Division of labor can enhance the fitness of interacting microorganisms via mechanisms that modulate growth rates or improve biomass yields (1-4). However, constraints on division of labor due to environmental context are largely undocumented. This knowledge gap includes division of labor strategies such as the exchange of organic acids. Secretion of organic acids in the presence of O_2, a phenotype often termed “overflow metabolism”, is a common microbial strategy for acclimating to stresses such as imbalances in electron donors and acceptors, imbalances in anabolic and catabolic nutrients, constrained cellular volume, and/or limited cellular surface area (5-11). The secreted organic acids can support food webs where microorganisms coexist in interdependent communities (12-18).

Cross-feeding organic acids has fitness costs for the producer such as the loss of potential cellular energy based on the properties of the exchanged metabolite. The accumulation of organic acids may inhibit the growth of both the producer and consumer due to cytosol acidification, membrane solubilization, or the reduction of thermodynamic driving forces necessary for chemical reactions (19-21). Organic acid exchange can also modulate consortia functioning via the relative rates of metabolite excretion and consumption. A consortium can display a ‘push’ metabolite interaction where the organic acid is secreted faster by the producer than imported by the consumer, or the consortium can demonstrate a ‘pull’ metabolite interaction where the consumer strain imports the metabolite at a comparable rate to its production (22, 23). Environmental context influences the fitness costs of organic acid exchange, yet these costs are poorly characterized especially for environments that are weakly buffered or acidic (24-26). These conditions are relevant to many natural habitats. For example, the pH of the human colon shifts dynamically from pH 5-8 as a function of axial position, reflecting the limited buffering capacity of colon contents and a dependency on local microbial metabolism (27). Additionally, aquatic ecosystems including estuarine and freshwater systems

bioRxiv preprint doi: https://doi.org/10.1101/2022.01.19.477024; this version posted January 21, 2022. The copyright holder for this preprint (which was not certified by peer review) is the author/funder, who has granted bioRxiv a license to display the preprint in perpetuity. It is made available under aCC-BY-NC-ND 4.0 International license.

have weak buffering capacities (28-30), though complex environments such as blood and some humic soils can have higher buffering capacities (31-33).

Natural microbial communities are often complex, comprised of hundreds or thousands of interacting species (34, 35), whereas synthetic consortia can be engineered to have a tractable number of defined phenotypes and interactions (21, 36, 37). Synthetic consortia can illuminate basic ecological properties and mechanisms of interaction that can be extrapolated to natural communities. The ability to control variables within synthetic communities also provides a powerful tool to investigate ecological theories (38). To this end, synthetic communities have been applied to problems of understanding the benefits of cooperation, the role of division of labor in the simultaneous utilization of different sugars, mechanisms for enhanced conversion of cellulose to biofuels, and the role of quorum sensing in coordinating consortial behavior, among others (1, 2, 19, 39, 40).

The presented study uses synthetic ecology to test two consortia interaction hypotheses. First, the study tests the role of environmental context, namely medium buffering capacity, on the fitness of consortia using division of labor strategies. Secondly, the study tests the effect of a push or pull metabolite exchanges on fitness when combined with environmental constraints. These hypotheses were evaluated by constructing two organic acid exchanging consortia: one consortium was based on acetic acid exchange (AAE) and the other on lactic acid exchange (LAE). Understanding the limits of division of labor strategies as a function of environment advances our understanding of consortia design principles essential for rational control of their catalytic potential.

RESULTS

Organic acids and culture pH are major mediators of growth inhibition. Protonated organic acids can diffuse across cellular membranes and inhibit cell growth (20, 41). Acetic and lactic

bioRxiv preprint doi: https://doi.org/10.1101/2022.01.19.477024; this version posted January 21, 2022. The copyright holder for this preprint (which was not certified by peer review) is the author/funder, who has granted bioRxiv a license to display the preprint in perpetuity. It is made available under aCC-BY-NC-ND 4.0 International license.

acids have different pK_a values (4.76 and 3.86, respectively) and different molecular weights (60 and 90 g mol^{-1}, respectively); both parameters influence the inhibitory properties of the organic acids (20). The inhibitory effects of acetic and lactic acids on wild type *E. coli* K12 MG1655 were quantified using two different contexts. First, the inhibitory properties of the organic acids were measured when the metabolites were present as the sole reduced carbon source in M9 medium and secondly, when the organic acids were present along with glucose in M9 medium (Fig. 1). The inhibitory properties were quantified using specific growth rate and plotted against (1) the total organic acid concentration ([HA + A^-], where HA is the protonated organic acid and A^- is the base) and (2) the protonated organic acid concentration only ([HA], calculated using the Henderson-Hasselbalch equation). Both acetic and lactic acid supported *E. coli* growth in M9 medium as the sole substrate; specific growth rates increased with increasing organic acid concentrations up to a critical threshold, after which further increases in organic acid reduced the specific growth rate. The maximum specific growth rate on acetic acid was ~0.23 h^{-1} at a total concentration of ~20 mM ([HA + A^-]), while the maximum specific growth rate on lactic acid was ~0.4 h^{-1} at a total concentration of ~100 mM (Fig. 1A). Acetic acid was more inhibitory than lactic acid on a total concentration basis (Fig. 1A). However, the protonated, uncharged form of the organic acids is a major mediator of inhibition due to enhanced diffusion across cellular membranes (20). When the specific growth rates were plotted as a function of the protonated organic acid concentrations ([HA]), lactic acid was more inhibitory than acetic acid at high concentrations (Fig. 1B).

Adding glucose (56 mM) to the M9 medium changed the metabolic role of acetic acid (Fig. 1C). *E. coli* preferentially consumed glucose as the carbon and energy source while acetic acid served as an inhibitor. The specific growth rates of the cultures in the presence of glucose and acetic acid never exceeded the specific growth rate of the glucose-only medium. However, mixtures of glucose and lactic acid increased the specific growth rates of the cultures over

bioRxiv preprint doi: https://doi.org/10.1101/2022.01.19.477024; this version posted January 21, 2022. The copyright holder for this preprint (which was not certified by peer review) is the author/funder, who has granted bioRxiv a license to display the preprint in perpetuity. It is made available under aCC-BY-NC-ND 4.0 International license.

129 glucose-only medium (Fig. 1C). The maximum specific growth rate (~0.73 h^{-1}) peaked at a total
130 lactic acid concentration of ~80 mM, after which the specific growth rate decreased. Acetic acid
131 was more inhibitory than lactic acid when examined on a total concentration basis in the
132 presence of glucose (Fig. 1C). However, examination of the data on a protonated acid basis
133 quantified the more inhibitory nature of lactic acid at higher concentrations (Fig. 1D).

134 pH and osmotic pressure were also investigated as separate environmental parameters. Growth
135 inhibition, quantified as culture specific growth rate, was measured for each variable. Specific
136 growth rate for *E. coli* cultures grown in M9 medium with glucose decreased sharply as the pH
137 was decreased (Fig. 1E). The specific growth rate was minimally affected over the tested range
138 of osmotic pressures, which represented 1 - 2.5X M9 salts with 56 mM glucose (Fig. 1F).

139 Organic acid and pH inhibition equations were parameterized using culturing data. A variety of
140 kinetic equations for modeling inhibitory compounds was tested (42). The best fit was selected
141 for each organic acid and condition (Table 1). Predicted values are plotted against experimental
142 data in Fig. 1B and 1D, while the results of all tested expressions and code can be found in the
143 supplementary material. Equations reported in the literature fit the culture properties for acetic
144 acid as the sole substrate, for combinations of acetic acid and glucose, and for lactic acid as the
145 sole substrate (42). Published equations did not fit the data well for combinations of lactic acid
146 and glucose, as the conventional expressions were not designed to reflect co-metabolism of
147 substrates in conjunction with inhibition. A dual substrate equation was incorporated with an
148 inhibition term to model the data. The resulting equation showed an improved fit to experimental
149 data (Fig. 1D, supplementary material).

150 A pH inhibition equation, separate from organic acids, was also fit to the experimental data
151 (Table 1). The parameterized equations considering organic acids, glucose, and pH were
152 combined into a predictive model for *E. coli* growth under multiple environmental stresses. The
153 model was tested with an independent experimental data set quantifying *E. coli* growth in the

bioRxiv preprint doi: https://doi.org/10.1101/2022.01.19.477024; this version posted January 21, 2022. The copyright holder for this preprint (which was not certified by peer review) is the author/funder, who has granted bioRxiv a license to display the preprint in perpetuity. It is made available under aCC-BY-NC-ND 4.0 International license.

presence of glucose with varying concentrations of acetate, different initial pH values, and different osmotic pressures. The predicted values matched the experimental data well, with a Pearson's correlation coefficient of 0.99 and corresponding p-value << 0.01 (supplementary material).

Producer-consumer consortia built to exchange either acetic or lactic acids. Acetic acid and lactic acid display different inhibitory properties, support different specific growth rates, confer different amounts of chemical energy, and require different enzymatic pathway investments for their production or consumption (Fig. 1, Fig. 2). Two *E. coli*-derived synthetic consortia were designed to test different organic acid exchange strategies hypothesized to change with both environmental context and interaction motif (push or pull metabolite exchange). The consortia were assembled by combining pairs of *E. coli* strains engineered for different phenotypes termed guilds: the producer guilds catabolized glucose and produced either acetic acid or lactic acid, and a consumer guild catabolized the organic acids (43, 44).

The producer guilds were designed for overflow phenotypes analogous to published metabolisms for either nitrogen- or iron-limited *E. coli* growth (45). The producer strain specializing in acetic acid secretion (ProdA) was created using four gene deletions (*ΔaceA ΔldhA ΔfrdA ΔatpF*). The *ΔatpF* gene deletion resulted in elevated substrate-level phosphorylation and high acetic acid secretion from glucose catabolism, analogous to other published systems (46, 47). A second producer guild specializing in lactic acid secretion (ProdL) had four respiration-associated operons deleted (*ΔcbdAB ΔcydAB ΔcyoABCD ΔygiN*) (48). The consumer strain consumed either acetic or lactic acid (ConsA/ConsL), but not glucose, and was constructed by deleting four genes associated with glucose transport and phosphorylation (*ΔptsG ΔptsM Δglk Δgcd*) (44). Wild type *E. coli* K12 MG1655 (WT) was used as the generalist guild for all comparisons. Monocultures of each guild were characterized in conventional M9 medium with their respective substrates to quantify their physiology (Table 2).

bioRxiv preprint doi: https://doi.org/10.1101/2022.01.19.477024; this version posted January 21, 2022. The copyright holder for this preprint (which was not certified by peer review) is the author/funder, who has granted bioRxiv a license to display the preprint in perpetuity. It is made available under aCC-BY-NC-ND 4.0 International license.

Catabolic efficiency and opportunity costs differ among the guilds. Cellular energy production was analyzed for all five guilds: 1) generalist (WT), 2) acetic acid producer (ProdA), 3) lactic acid producer (ProdL), 4) consumer based on acetic acid oxidation (ConsA), and 5) consumer based on lactic acid oxidation (ConsL) using a published *E. coli* metabolic model (Fig. 2, (49, 50), supplementary material). ProdA produced 4 mol ATP (mol glucose)$^{-1}$ while ProdL produced 2 mol ATP (mol glucose)$^{-1}$. ProdA extracted more energy from glucose via substrate-level phosphorylation using the Pta enzyme. The exchanged organic acids have the same degree of reduction (4 electron mols Cmol^{-1}) but different chemical energies (quantified here as enthalpy of combustion ($\Delta H_c°$) = 875 and 1362 kJ mol^{-1} for acetic acid and lactic acid, respectively), largely due to the difference in the molecular weights of the molecules. Additionally, the molecules entered central metabolism at different positions, influencing their potential for substrate level phosphorylation. ConsA and ConsL produced 7 and 12 mol ATP (mol organic acid)$^{-1}$, respectively. The *in silico* model of the WT generalist produced 26 mol ATP (mol glucose)$^{-1}$ when the substrate was completely oxidized (Fig. 2, supplementary material).

Cross feeding byproducts, such as organic acids, necessarily entails opportunity costs for the producer guild. Here, opportunity costs are a quantification of benefits not realized by a cell due to use of a particular phenotype (5, 22). The exchange of a reduced metabolite precluded its use by the producer guild for other functions such as cellular energy generation. Opportunity costs were quantified based on cellular energy that was not generated due to metabolite secretion (49, 50) (Fig. 2, supplementary material). The opportunity cost for ProdA was 22 mol ATP (mol glucose)$^{-1}$ while the opportunity cost for ProdL was 24 mol ATP (mol glucose)$^{-1}$.

Proteomic investment costs for each guild were heavily influenced by a few enzymatic steps. Metabolic phenotypes require the assembly of the necessary proteomes (49, 50). An *in silico* analysis quantified the amino acid requirements to realize the core proteomes of the five guilds. *In silico* analysis considered the minimum proteome proxy for modeling the relationship

bioRxiv preprint doi: https://doi.org/10.1101/2022.01.19.477024; this version posted January 21, 2022. The copyright holder for this preprint (which was not certified by peer review) is the author/funder, who has granted bioRxiv a license to display the preprint in perpetuity. It is made available under aCC-BY-NC-ND 4.0 International license.

between flux and enzyme concentration, as described previously (49, 50). This proxy assumes that the concentration of all central metabolism enzymes can be approximated by the relationship $[E_i]/[E_j] \sim 1$; this proxy has been applied with notable successes in *E. coli* as well as other microbial species (50, 51).

The generalist, with its complete oxidation metabolism, required the largest total proteome investment of ~97,000 amino acids although it had the smallest proteome investment per ATP produced at 3,906 amino acids ATP^{-1} (Fig. 2). In descending order based on total investment, ConsL had an investment cost of ~85,000 amino acids (7,471 amino acids ATP^{-1}), ProdA required ~59,000 amino acids (15,856 amino acids ATP^{-1}), ConsA required ~44,000 amino acids (8,175 amino acids ATP^{-1}), and finally ProdL required the smallest investment of ~14,000 amino acids (6,831 amino acids ATP^{-1}). The pyruvate dehydrogenase complex (PDHc, 42,096 amino acids per complex), which oxidizes pyruvate to acetyl-CoA, had a large influence on the investment cost for WT, ConsL, and ProdA (49, 50). The investment cost from this enzyme was avoided by the ConsA and ProdL guilds. There was also a large investment cost associated with the citric acid cycle due to the α-ketoglutarate dehydrogenase complex and the electron transport chain enzymes (supplementary material).

The different guilds have different core proteomes that catabolize different substrates with different metabolic efficiencies complicating inter-guild comparisons. Therefore, the proteome investment required for each guild was converted into ATP equivalents using the guild-specific *in silico* models ((52), supplementary material). The Cmols of substrate required for each guild to assemble the core proteome were calculated; this quantity of substrate was converted into an equivalent number of ATP using the guild-specific Cmol substrate $(mol\ ATP)^{-1}$ yield. The proteome resource requirements were calculated as a total investment of ATP equivalents to construct the proteome and additionally, this investment was normalized to the number of ATP produced per core metabolism (Fig. 2). The WT proteome had the most efficient ratio of

bioRxiv preprint doi: https://doi.org/10.1101/2022.01.19.477024; this version posted January 21, 2022. The copyright holder for this preprint (which was not certified by peer review) is the author/funder, who has granted bioRxiv a license to display the preprint in perpetuity. It is made available under aCC-BY-NC-ND 4.0 International license.

proteome investment per ATP produced (99,890 ATP equivalents (ATP produced) $^{-1}$), followed by ProdL, ProdA, ConsL, and finally ConsA which required a proteome investment equivalent to 234,899 ATPs to produce an ATP.

Experimental properties of organic acid exchanging consortia. Batch growth properties of the producer guilds were measured as monocultures and as cocultures with the consumer guild. Glucose was the sole reduced carbon source in the modified M9 medium, and four initial pH values were tested (6.0, 6.5, 7.0, and 7.5). The modified M9 medium contained 6.3 mM total phosphate to represent a low buffering capacity environment. WT monocultures served as generalist controls.

WT monocultures produced the highest final biomass titer and displayed the highest specific growth rate at an initial pH of 7.0 (Fig. 3A, 3B). The cultures grown with an initial pH of 7.5 had the slowest specific growth rate (Fig. 3B). Medium pH decreased with biomass accumulation for all four initial pH values (Fig. 3C). The WT cultures accumulated acetic acid consistent with an *E. coli* overflow metabolism (Fig. 3D). Growth data and calculated rates for all conditions and guilds are provided in the supplementary material.

Acetic acid-exchanging consortium displayed a push interaction motif. Biomass titers for the acetic acid-exchanging (AAE) consortium changed with initial medium pH (Fig. 4A). The highest biomass titer occurred when the initial pH of the medium was 7.5, whereas the highest specific growth rate occurred when the initial pH of the medium was 7.0 (Fig. 4A, 4B). The consortium growth rate was an aggregate rate comprised of the ProdA and ConsA growth rates and was slower than the ProdA monoculture (Fig. 4B, Table 2). The culture pH decreased with time in trends proportional to biomass production with a final pH range of 4.1 – 4.5 (Fig. 4C). The AAE consortium accumulated 50% more biomass relative to ProdA monocultures at initial pH values of 6.0 and 7.5, quantifying a benefit of guild interactions within the tested environs (Fig. 4D).

bioRxiv preprint doi: https://doi.org/10.1101/2022.01.19.477024; this version posted January 21, 2022. The copyright holder for this preprint (which was not certified by peer review) is the author/funder, who has granted bioRxiv a license to display the preprint in perpetuity. It is made available under aCC-BY-NC-ND 4.0 International license.

The rate of acetic acid secretion by ProdA exceeded the rate of consumption by ConsA (Fig. 4E), resulting in organic acid accumulation and a cellular interaction motif termed here as a metabolite 'push'. The presence of ConsA did not result in the complete consumption of secreted acetic acid due to low pH and high concentrations of acetic acid arresting guild growth. The cellular ratio of the two guild members was measured as a function of initial pH and cultivation time (Fig. 4F). The cellular ratio was approximately 1 ProdA : 1 ConsA at the cessation of growth regardless of the initial pH.

Lactic acid-exchanging consortium displayed a pull interaction motif. Batch growth of the lactic acid-exchanging (LAE) consortium produced the highest biomass titers when the initial pH of the medium was 7.0 or 7.5 (Fig. 5A). The highest specific growth rates occurred when the initial pH of the medium was 6.5 and 7.0 (Fig. 5B). Culture pH decreased continuously with time to a final endpoint of ~4, except for the LAE consortium which had an initial pH of 7.5 (Fig. 5C). The pH of this culture initially decreased to ~5 before recovering to ~6.8. This property was analyzed in more detail in later sections. The LAE consortium had substantially higher biomass titers and biomass per glucose yields as compared to ProdL monocultures (Fig. 5D). In contrast to the AAE consortium, the LAE consortium grew faster than the ProdL monoculture, likely due to the high ConsL specific growth (Table 2).

The LAE consortium had balanced rates of lactic acid secretion and consumption, resulting in low accumulation of the organic acid (Fig. 5E). The consortial interaction template was termed a metabolite 'pull' mechanism because ConsL imported the organic acid at rates comparable to the ProdL secretion rates. The secreted lactic acid was nearly exhausted by the end of the growth phase; any remaining lactic acid was consumed during stationary phase. Selective agar plating quantified the cellular ratios of the ProdL and ConsL guilds (Fig. 5F). The producer ratio decreased during growth, reaching an average ratio of 5 ProdL : 95 ConsL by stationary phase.

bioRxiv preprint doi: https://doi.org/10.1101/2022.01.19.477024; this version posted January 21, 2022. The copyright holder for this preprint (which was not certified by peer review) is the author/funder, who has granted bioRxiv a license to display the preprint in perpetuity. It is made available under aCC-BY-NC-ND 4.0 International license.

LAE consortium properties vary as a function of initial cell ratios. The properties of the LAE consortium were studied for pH robustness and optimality of biomass titer. Different initial cellular ratios of ProdL : ConsL were tested (1:1, 10:1, 100:1, 1:2) using an initial medium pH of 7.0 and 7.5. For these experiments, ProdL was inoculated at the same concentration as the preceding 1:1 cell ratio experiments (Fig. 5), while the ConsL concentration was adjusted to achieve the desired cell ratios. This design resulted in a near constant volumetric lactic acid production rate across the conditions, with the primary experimental change being the ConsL cell concentration.

The consortium behavior was sensitive to the initial conditions. Biomass titers were highest for an initial 1:1 guild ratio and an initial pH of 7.0 (Fig. 6A); however, this condition did not exhibit a pH recovery trend. Different initial guild ratios were required to induce the pH recovery trend when the initial pH was 7.0 (Fig. 6B). Cultures with either higher or lower ProdL : ConsL cell ratios (100:1, 10:1, 1:2) modulated the pH trajectory after an early pH decrease, demonstrating a pH recovery phase corresponding to lactic acid consumption (Fig. 6B). Minimal, transient accumulation of lactic acid was observed before its subsequent consumption (Fig. 6C). Small amounts of acetic acid accumulated during the pH 7.5 experiments (Fig 6E, supplementary material). The consumer was postulated to convert the lactic acid into acetic acid, which was then later consumed in a diauxic manner. ConsL dominated the consortium by the end of batch growth for all tested conditions (Fig. 6D).

Due to the slow growth rate during the pH recovery phase, the LAE consortium experiments lasted up to two weeks. Abiotic controls quantified the role of evaporation on medium volume and changes in pH (supplementary material). Evaporation accounted for less than a 10% change in liquid volume and did not result in a change to the medium pH.

Consortium fitness was a function of environmental context. The synthetic consortia properties were compared to the WT generalist to quantify advantages and disadvantages of

bioRxiv preprint doi: https://doi.org/10.1101/2022.01.19.477024; this version posted January 21, 2022. The copyright holder for this preprint (which was not certified by peer review) is the author/funder, who has granted bioRxiv a license to display the preprint in perpetuity. It is made available under aCC-BY-NC-ND 4.0 International license.

the different metabolite exchange templates. Six metrics of fitness were quantified: 1) final biomass titer, 2) total glucose catabolized, 3) biomass produced per glucose consumed, 4) biomass produced per H^+ accumulated, 5) accumulation of byproducts, and 6) specific growth rate.

The AAE consortium did not outperform the WT generalist in any considered fitness metric, though the biomass per glucose yields of the AAE consortium and generalist were equivalent when the initial medium pH was 7.0 or 7.5.

The LAE consortium outperformed the WT generalist at four of the six fitness metrics for a starting pH of 7.0. The LAE consortium produced 55% more total biomass, consumed 86% more glucose, and produced 51% more biomass per H^+ secreted as compared to the WT generalist (Fig. 7A, 7B, 7C). Additionally, the LAE consortium had minimal byproducts at stationary phase whereas the WT culture accumulated ~2.5 mM of acetic acid. The LAE consortium and WT cultures had comparable biomass per glucose yields (Fig. 7D); however, the WT generalist grew faster (0.53 vs. 0.22 h^{-1}) than the LAE consortium (Fig. 3B and Fig. 5B).

The performance of the LAE consortium was also compared to the WT generalist when grown in M9 medium with a conventional 64 mM phosphate buffer and an initial pH of 7.0. Increasing the buffering capacity kept the medium pH ≥ 6.2 for the WT cultures and ≥ 6.8 for the LAE cultures, which reduced the fitness cost of accumulating organic acids. The buffered environment altered the competitive properties of the LAE consortium relative to the WT generalist (Fig. 8). The WT generalist had superior properties in five of the six fitness metrics (the LAE consortium had no measurable byproduct accumulation at stationary phase), highlighting the environmental context-dependent nature of competitive microbial interactions and optimal consortia design principles.

bioRxiv preprint doi: https://doi.org/10.1101/2022.01.19.477024; this version posted January 21, 2022. The copyright holder for this preprint (which was not certified by peer review) is the author/funder, who has granted bioRxiv a license to display the preprint in perpetuity. It is made available under aCC-BY-NC-ND 4.0 International license.

Ordinary differential equation (ODE) models were developed to further test the fitness properties of the consortia and WT cultures at an initial pH of 7.0 (supplementary material). Experimentally measured rate and yield parameters from monoculture producer, consumer, and generalist guilds were used to parameterize the model. Model predictions for monocultures and consortia were compared with experimental measurements of biomass, pH change, substrate consumption, and organic acid accumulation and showed remarkably similar patterns. Most notably, simulations demonstrated the observed differences between the low and high buffered medium for the WT cultures and LAE consortium (supplementary material). The cross-validation further emphasizes the importance of environmental context in dictating the competitiveness of consortia interactions.

DISCUSSION

Two synthetic *E. coli* consortia were constructed to test principles governing microbial interactions. The consortia were designed to catabolize glucose and unidirectionally exchange either acetic or lactic acid. Collectively, each consortium had the same genomic potential as wild type *E. coli* K-12 since the genes deleted in one guild were present in the other guild. However, the two consortia displayed very different growth properties based on the partitioning of key genes. The LAE consortium outperformed the WT based on four of six considered fitness metrics, including the production of 55% more total biomass, the consumption of 86% more glucose, and the production of 51% more biomass per H^+ secreted as compared to the WT (Fig. 7A, 7B, 7C). Additionally, the LAE consortium consumed all reduced byproducts by stationary phase, while the WT accumulated substantial acetic acid (Fig. 3, 5, 7). These fitness advantages came with the tradeoff of a slower growth rate.

Synthetic consortia with defined components provide the basis for testing hypotheses and extracting design principles for community interactions. The first design principle central to the enhanced consortium properties observed in this study was the relationship between the

bioRxiv preprint doi: https://doi.org/10.1101/2022.01.19.477024; this version posted January 21, 2022. The copyright holder for this preprint (which was not certified by peer review) is the author/funder, who has granted bioRxiv a license to display the preprint in perpetuity. It is made available under aCC-BY-NC-ND 4.0 International license.

relative rates of secretion and uptake of exchanged metabolites, e.g. push vs. pull interaction motifs (53). The pull interaction motif used by the LAE consortium was sufficient to prevent substantial accumulation of the inhibitory metabolite, which created a benefit for both the consumer and producer. The balance of organic acid production and consumption in the LAE consortium modulated the environmental pH, which delayed the growth-arresting effects of accumulated organic acid and low pH experienced by the WT. A second consortial design rule gleaned from this study illustrated that no metabolite exchange is without cost for the producer; there are opportunity costs associated with uncaptured energy and often byproduct inhibition (54) (Fig. 1, Fig. 2). However, the opportunity cost for the producer guild can be off set through increased flux of glucose if consortial interactions can ameliorate the increase in organic acid secretion. The ProdL guild had a higher opportunity cost (24 mol ATP (mol glucose)$^{-1}$) than the ProdA guild (22 mol ATP (mol glucose)$^{-1}$) but the LAE consortium outperformed the AAE consortium due largely to the metabolite pull mechanism.

A third design principle demonstrates that environmental context such as buffering capacity dictates which metabolite exchange strategy, if any, will result in a competitive advantage for participants (55). Low buffering capacity is common in natural environments (27-30). The LAE consortium exhibited many enhanced fitness metrics relative to the WT under low buffering conditions. Consistent with the thought experiment of the Darwinian Demon, which states it is not possible to optimize all fitness behaviors simultaneously (56), the LAE consortium had a reduced growth rate compared to the WT. Fast growth rates are major drivers of fitness in well-mixed, spatially homogenous, laboratory environments where cultures are often supplied with abundant nutrients. In nutrient poor environments, growth rates are reduced and the benefits of enhanced substrate depletion, enhanced biomass accumulation, and reduced H^+ production are likely important fitness metrics. The current study demonstrates that changing the buffering capacity changes the fitness of different phenotypes. The WT outperformed the LAE consortium

bioRxiv preprint doi: https://doi.org/10.1101/2022.01.19.477024; this version posted January 21, 2022. The copyright holder for this preprint (which was not certified by peer review) is the author/funder, who has granted bioRxiv a license to display the preprint in perpetuity. It is made available under aCC-BY-NC-ND 4.0 International license.

when a conventional phosphate buffering capacity (64 vs. 6.3 mM) was used. Enhanced buffering capacities also alter the fitness afforded by acetic acid exchange. A previous study measured a 15% enhancement in biomass productivity in an alternative acetic acid-exchanging *E. coli* consortium (44). The acetic acid producing strain in that study secreted approximately 10% of the glucose carbon as acetic acid compared to 30-50% in the current study. Tuning the secretion rate to the consumption rate is an important design parameter that could be optimized using genetic engineering or adaptive evolution.

Nutrient limitation is a common environmental challenge (57). Overflow phenotypes, where reduced byproducts are secreted in the presence of external electron acceptors, can be competitive acclimations to nutrient limitation (49). As demonstrated in Fig. 2, abridged central metabolism pathways require fewer resources to construct but only partially oxidize substrates, highlighting the tradeoff between metabolic pathway investment into proteins and the opportunity cost quantified by carbon source oxidation efficiency. Wild type *E. coli* secretes different organic acids, including acetic and lactic acids, in different quantities as a function of different nutrient limitations and different degrees of nutrient stress (45). The secretion of reduced byproducts in chemostats can lead to the evolution of cross-feeding populations with higher biomass titers (4) likely due to a combination of factors highlighted here, including more biomass per H^+ as well as the nonlinear relationship between enzyme velocity and the total required resource investment (enzymes and metabolites) to achieve that velocity (22, 43, 58, 59). This biomass yield benefit can potentially be realized in consortia without spatial segregation of populations (60).

The growth of each culture was arrested at a pH of 4.1-4.5 regardless of the initial pH. The pH decrease was primarily the result of two processes: organic acid secretion followed by H^+ dissociation and secondly, the consumption of ammonium for biomass synthesis, which released an H^+ when the nitrogen source was incorporated into biosynthetic molecules as

bioRxiv preprint doi: https://doi.org/10.1101/2022.01.19.477024; this version posted January 21, 2022. The copyright holder for this preprint (which was not certified by peer review) is the author/funder, who has granted bioRxiv a license to display the preprint in perpetuity. It is made available under aCC-BY-NC-ND 4.0 International license.

ammonia. Thus, biomass production itself contributed to reaching the critical pH threshold. The WT drove the pH to the critical level via a combination of biomass production and acetic acid secretion. The LAE consortium, however, did not accumulate substantial organic byproducts, allowing more biomass to be produced before reaching the critical pH threshold.

Exchange of organic acids in microbial consortia can also be analyzed from the perspective of other ecological principles that are typically applied at the macro-scale. For example, the resource ratio theory suggests that two populations can cooperate to improve overall efficiency of resource usage. As an alternative to the competitive exclusion principle, it has been proposed that cooperating populations can exchange resources that they are each more efficient at utilizing and thereby more effectively deplete total resources (61). The two synthetic consortia effectively partitioned glucose and O_2 between two different populations. The ProdL guild was constructed by deleting the primary respiration chain enzymes including the O_2 cytochromes (48). ConsL required the external electron acceptor O_2 for the complete oxidation of the organic acid. The lactic acid exchanged between the consortium members drove the glucose concentration lower than the WT generalist; while not measured directly, it is proposed that the high biomass concentration in the LAE consortium drove the O_2 levels lower than the WT cultures. This performance would potentially classify the LAE consortium as a “super-competitor unit” as defined by de Mazancourt & Schwartz (61).

CONCLUSION

The presented work used synthetic consortia to test hypotheses governing microbial interactions mediated by push or pull metabolite exchange, quantified the inhibitory properties of the exchanged metabolites, calculated the opportunity costs associated with different phenotypes, and demonstrated the powerful role of environmental context on consortia performance. Ultimately, environment constrains whether division of labor strategies can enhance or decrease the fitness of participants.

bioRxiv preprint doi: https://doi.org/10.1101/2022.01.19.477024; this version posted January 21, 2022. The copyright holder for this preprint (which was not certified by peer review) is the author/funder, who has granted bioRxiv a license to display the preprint in perpetuity. It is made available under aCC-BY-NC-ND 4.0 International license.

MATERIALS AND METHODS

Culturing media. Two different variations of M9 media were used. Conventional M9 medium for characterizing strain growth (62) contained 6 g L^{-1} Na_2HPO_4 (42 mM), 3 g L^{-1} KH_2PO_4 (22 mM), 1 g L^{-1} NH_4Cl, and 0.5 g L^{-1} NaCl. After autoclaving, 1 mL L^{-1} 1 M $MgSO_4 \cdot 7H_2O$ solution was added along with 1 mL L^{-1} trace metals solution, containing (per L): 0.73 g $CaCl_2 \cdot 2H_2O$, 0.10 g $MnCl_2 \cdot 4H_2O$, 0.17 g $ZnCl_2$, 0.043 g $CuCl_2 \cdot 2H_2O$, 0.06 g $CoCl_2 \cdot 6H_2O$, 0.06 g $Na_2MoO_4 \cdot 2H_2O$, and 0.24 g $FeCl_3 \cdot 6H_2O$. Carbon source (glucose, sodium acetate, or sodium lactate) was added to achieve the desired concentration from a filter sterilized stock solution. The pH of the medium was adjusted, if necessary, with HCl or NaOH and the medium then filter sterilized. For experiments investigating pH effect, conventional M9 medium was modified to ensure carbon limitation at 5 g L^{-1} glucose by increasing nitrogen, iron, and sulfate content. Modified M9 medium contained 2.5 g L^{-1} NH_4Cl, 1.5 mL L^{-1} 1 M $MgSO_4 \cdot 7H_2O$, and an additional 2.4 mg L^{-1} $FeCl_3 \cdot 6H_2O$. Low phosphate modified M9 medium contained 0.9 g L^{-1} Na_2HPO_4 (6.3 mM) and no KH_2PO_4.

Strains. Mutant strains were derived from *E. coli* str. K-12 substr. MG1655. The wildtype strain served as the metabolic generalist for comparison with the mutant specialist strains.

Producer guild strains. The lactate producer strain, *E. coli* str. ECOM4LA, was obtained from the Pålsson group (48). The strain was designed to prevent O_2 uptake through deletions of three terminal oxidases (*cbdAB*, *cydAB*, and *cyoABCD*), as well as deletion of the quinol monooxygenase *ygiN*; O_2 consumption was reduced ~60-fold and considered negligible. The strain was received in a frozen glycerol stock. Growth of the initial stock was slow, possibly due to freeze-thaw cycles. Thus, the stock was serially passaged by transferring during exponential growth phase to fresh conventional M9 media containing 4 g L^{-1} glucose. Samples were tested for growth rate periodically, and serial passaging was continued until growth rate plateaued (~120 generations).

bioRxiv preprint doi: https://doi.org/10.1101/2022.01.19.477024; this version posted January 21, 2022. The copyright holder for this preprint (which was not certified by peer review) is the author/funder, who has granted bioRxiv a license to display the preprint in perpetuity. It is made available under aCC-BY-NC-ND 4.0 International license.

The acetate producer, *E. coli* str. 409, was constructed from *E. coli* str. 307G100 *(ΔaceA*, Δ*ldhA*, Δ*frdA*) which was designed in a previous study (44). An additional deletion (*atpF*) was added to *E. coli* str. 307G100 using P1 viral transduction with the KEIO mutant library according to (37). *E. coli* str. 409 was designed to function similarly to the homoacetate producing strain reported in Causey et al. (46). The *atpF* gene deletion was confirmed with PCR (forward primer 5'-GTTATGGGTCTGGTGGATGC-3', reverse primer 5'-CGAACACCAAAGTGTAGAACGC-3').

Consumer guild strain. The consumer strain, *E. coli* str. 403, was previously constructed (44) to prevent glucose consumption by blocking the glucose phosphotransferase uptake system and phosphorylation of glucose via *ptsG*, *ptsM*, *glk*, and *gcd* deletions. This strain does not grow readily on glucose as the sole carbon source but is able to metabolize glucose at a slow base rate (0.016 h^{-1}), whereas lactate and acetate are readily consumed in the presence of O_2.

Batch culturing. All cultures were grown at 37°C in a shaking incubator at 150 rpm. Frozen stock vials prepared from the same culture were used for all experiments. *E. coli* MG1655 and producer strain inocula were grown with 5 g L^{-1} glucose as the carbon source, and consumer strain inocula were grown with either 1 g L^{-1} sodium acetate or 2.8 g L^{-1} sodium lactate. Disposable test tubes containing 5 mL modified M9, pH 7.0, were inoculated from frozen stock and incubated until optical density at 600 nm (OD_{600}) reached 0.2 – 0.4. Cultures were transferred into 25 mL modified M9, pH 7.0, in 250-mL borosilicate glass baffled shake flasks to an initial OD_{600} ~0.010 and grown until OD_{600} reached 0.2 – 0.4. Sufficient culture for inoculation was aliquoted into 15-mL Falcon tubes and pelleted at 4000 rpm for 10 minutes at 20°C. Cells were washed in an equal volume of low phosphate modified M9 containing 5 g L^{-1} glucose to remove metabolic byproducts and excess phosphate and were pelleted again. 100 mL experimental batch cultures of low phosphate modified M9 containing 5 g L^{-1} glucose were inoculated to an initial OD_{600} ~0.020. 500-mL borosilicate glass baffled shake flasks with silicone sponge closures were used to allow gas exchange with minimal evaporation. Consortia were

bioRxiv preprint doi: https://doi.org/10.1101/2022.01.19.477024; this version posted January 21, 2022. The copyright holder for this preprint (which was not certified by peer review) is the author/funder, who has granted bioRxiv a license to display the preprint in perpetuity. It is made available under aCC-BY-NC-ND 4.0 International license.

476 inoculated to an initial OD_{600} ~0.020 of producer and consumer each (to provide the same
477 density of primary glucose-consuming strain in all conditions).

478 Flasks were sampled aseptically approximately every doubling time; total culture volume was
479 not reduced more than 20% by the end of the experiment. OD_{600} and pH were measured, and
480 culture supernatant was frozen at -20°C for subsequent metabolite analysis. For consortia
481 experiments, samples were also analyzed for producer and consumer populations. Samples
482 were serially diluted 1:10 in phosphate buffered saline (PBS; 42.5 mg L^{-1} KH_2PO_4 and 405.5 mg
483 L^{-1} $MgCl_2 \cdot 6H_2O$) and drop plated (10 10-µL drops) on selective conventional M9 agar after the
484 method of (63). Selective plates contained 15 g L^{-1} Noble agar (Affymetrix) to eliminate bacterial
485 growth on carbon source contaminants available in the agar. The consumer was selected with
486 either 1 g L^{-1} sodium lactate or 1 g L^{-1} sodium acetate, and the producer was selected with 1 g L^{-1}
487 glucose. In the lactate consortia experiments, both consumer and producer were found
488 capable of growth on glucose agar plates due to the slower relative growth rate of the producer
489 and the high yield of lactate. Therefore, the producer proportion of the population was estimated
490 by subtracting the consumer counts on lactate agar from the total population (producer and
491 consumer) counts on glucose agar. Experiments were performed with triplicate flasks for each
492 condition along with an un-inoculated control flask carried through the entire inoculation and
493 sampling procedure.

494 **Dry weight and colony-forming unit correlations.** Correlation of OD_{600} to cell dry weight
495 (cdw) was determined for the producer and consumer strains separately. Producer strains were
496 grown in conventional M9 containing 4 g L^{-1} glucose, and the consumer strain was grown in
497 conventional M9 containing 2.8 g L^{-1} lactate. Exponentially growing cultures were harvested on
498 ice, pelleted at 4000 rpm for 20 minutes at 4°C in 50-mL Falcon tubes, re-suspended in an
499 equal volume of carbon-free M9 to minimize lysis of cells, and pelleted again. The cultures were
500 combined and concentrated into one tube, and a series of 12 dilutions ranging from OD_{600} 0.25

bioRxiv preprint doi: https://doi.org/10.1101/2022.01.19.477024; this version posted January 21, 2022. The copyright holder for this preprint (which was not certified by peer review) is the author/funder, who has granted bioRxiv a license to display the preprint in perpetuity. It is made available under aCC-BY-NC-ND 4.0 International license.

501 to 2.5 was made using carbon-free M9 as the diluent. OD_{600} of each dilution was measured and
502 recorded, and 5 mL of each dilution was aliquoted into a pre-dried and pre-weighed aluminum
503 pan. Three aluminum pans contained 5 mL carbon-free M9 as a media control. Pans were
504 placed in a drying oven at 80°C for 24 h and weighed. Samples were dried for an additional 24 h
505 and weighed again to ensure that samples were completely dry. Biomass concentration was
506 calculated from the difference in mass. Correlation curves were constructed by setting the mass
507 of the media control as zero and adjusting the sample masses accordingly. The cdw correlation
508 for *E. coli* MG1655 was obtained from (64).

509 Colony-forming unit (CFU) to OD_{600} correlation curves were constructed in a similar manner.
510 Exponentially growing cultures were harvested and a series of eight dilutions was made,
511 ranging from OD_{600} 0.010 – 0.275 for *E. coli* str. ECOM4LA and 0.010 – 1.1 for *E. coli* str. 403.
512 OD_{600} was measured and recorded, and each dilution was serially diluted 1:10 in PBS and drop
513 plated on LB agar (63). Plates were incubated overnight, counts from appropriate dilutions (3-30
514 colonies within a drop) were recorded, and CFU mL^{-1} values were calculated.

515 **Metabolite analysis.** Glucose consumption and organic acid secretion were monitored via high-
516 performance liquid chromatography (HPLC). An Agilent 1200 HPLC instrument was used with
517 filtered (0.22 µm) 5 mM sulfuric acid as the mobile phase. Samples were stored in a chilled
518 (4°C) autosampler during the run, and 20 µL sample injections were run on a Bio-Rad HPX-87H
519 column operated at 45°C. Glucose was detected with refractive index detector (RID) with heater
520 set at 40°C, and concentrations were normalized by fucose. Organic acids acetate and lactate
521 were detected with variable wavelength detector (VWD). Cells were pelleted from samples and
522 supernatant was frozen at -20°C until analysis, before which samples were filtered (0.45 µm)
523 and prepared 1:1 (v/v) with 2x mobile phase containing fucose as an internal standard.
524 Concentrations were quantified using calibration curves with limit of detection at 0.1 mM.

bioRxiv preprint doi: https://doi.org/10.1101/2022.01.19.477024; this version posted January 21, 2022. The copyright holder for this preprint (which was not certified by peer review) is the author/funder, who has granted bioRxiv a license to display the preprint in perpetuity. It is made available under aCC-BY-NC-ND 4.0 International license.

Formate and succinate standards were also measured, but significant levels were not detected in the samples.

Kinetic expression modeling. A compendium of possible kinetic expressions to describe the inhibition effect of organic acids was identified (42) and examined against the lactate and acetate inhibition data both with and without glucose. Additionally, dual substrate models were explored to improve model fit for data with both glucose and lactate present in the medium (65), given the observation of co-consumption of the two compounds. Equations and parameters were defined in Python and the data were fit using the Levenberg-Marquardt algorithm in the SciPy library (scipy.org). Goodness-of-fit was assessed both visually and with the chi-square test function in SciPy. The Python fitting routines used are included in the supplementary material.

To model the dynamics of consortia growth compared to producer and generalist monocultures, a set of ordinary differential equations describing growth, substrate and product concentrations, and pH, (based on acidification by organic acid byproducts and using a scaling factor to compensate for protons contributed by consumption of ammonium) was developed based on Monod kinetics. The ode45 solver in MATLAB to simulate batch growth. The model files and parameters used (derived from experimental data for the individual producer and consumer monocultures) are included in the supplementary material.

Metabolic modeling. A published *E. coli* central metabolism model was used to quantify the metabolic efficiencies of the guilds (49, 50). Distinct guild models were created by inactivating the appropriate reactions. The *in silico* model was decomposed into elementary flux modes using CellNetAnalyzer v.2018.1 (66), and individual elementary flux modes were identified using Excel and the noted optimization criteria. The *in silico* model can be found in the supplementary material.

bioRxiv preprint doi: https://doi.org/10.1101/2022.01.19.477024; this version posted January 21, 2022. The copyright holder for this preprint (which was not certified by peer review) is the author/funder, who has granted bioRxiv a license to display the preprint in perpetuity. It is made available under aCC-BY-NC-ND 4.0 International license.

549 **ACKNOWLEDGEMENTS**

550 The study was supported by NSF awards DMS 1361240 and DGE 0654336, and NIH award
551 U01EB019416. A.E.B. was supported in part by the USDA National Institute of Food and
552 Agriculture (Hatch 1018813) and the M.J. Murdock Charitable Trust Biology Start-up Grant to
553 Carroll College. Undergraduate researchers. K.P., A.S., T.J., A.B., M.D. were supported in part
554 by the Montana State Undergraduate Scholars program and the National Institute of General
555 Medical Sciences of the National Institutes of Health under Award Number P20GM103474. The
556 content is solely the responsibility of the authors and does not necessarily represent the official
557 views of the National Institutes of Health. The authors would also like to thank the Pålsson
558 research group for the gift of the ECOM4LA strain.

559

560

bioRxiv preprint doi: https://doi.org/10.1101/2022.01.19.477024; this version posted January 21, 2022. The copyright holder for this preprint (which was not certified by peer review) is the author/funder, who has granted bioRxiv a license to display the preprint in perpetuity. It is made available under aCC-BY-NC-ND 4.0 International license.

REFERENCES

1. Pande S, Merker H, Bohl K, Reichelt M, Schuster S, de Figueiredo LF, Kaleta C, Kost C. 2014. Fitness and stability of obligate cross-feeding interactions that emerge upon gene loss in bacteria. The ISME Journal 8:953-962.
2. Mee MT, Collins JJ, Church GM, Wang HH. 2014. Syntrophic exchange in synthetic microbial communities. Proc Natl Acad Sci U S A 111:E2149-56.
3. Wintermute EH, Silver PA. 2010. Emergent cooperation in microbial metabolism. Molecular Systems Biology 6:407.
4. Rosenzweig RF, Sharp RR, Treves DS, Adams J. 1994. Microbial evolution in a simple unstructured environment: genetic differentiation in Escherichia coli. Genetics 137:903-917.
5. Carlson RP, Beck AE, Phalak P, Fields MW, Gedeon T, Hanley L, Harcombe WR, Henson MA, Heys JJ. 2018. Competitive resource allocation to metabolic pathways contributes to overflow metabolisms and emergent properties in cross-feeding microbial consortia. Biochemical Society Transactions 46:269-284.
6. Molenaar D, van Berlo R, de Ridder D, Teusink B. 2009. Shifts in growth strategies reflect tradeoffs in cellular economics. Mol Syst Biol 5:323.
7. Bruggeman FJ, Planque R, Molenaar D, Teusink B. 2020. Searching for principles of microbial physiology. FEMS Microbiol Rev 44:821-844.
8. Shimizu K. 2016. Metabolic Regulation and Coordination of the Metabolism in Bacteria in Response to a Variety of Growth Conditions. Adv Biochem Eng Biotechnol 155:1-54.
9. Szenk M, Dill KA, de Graff AMR. 2017. Why Do Fast-Growing Bacteria Enter Overflow Metabolism? Testing the Membrane Real Estate Hypothesis. Cell Syst 5:95-104.
10. Zhuang K, Vemuri GN, Mahadevan R. 2011. Economics of membrane occupancy and respiro-fermentation. Mol Syst Biol 7:500.
11. Ramsey MM, Rumbaugh KP, Whiteley M. 2011. Metabolite cross-feeding enhances virulence in a model polymicrobial infection. PLoS Pathog 7:e1002012.
12. Wang T, Goyal A, Dubinkina V, Maslov S. 2019. Evidence for a multi-level trophic organization of the human gut microbiome. PLoS Comput Biol 15:e1007524.
13. Zelezniak A, Andrejev S, Ponomarova O, Mende DR, Bork P, Patil KR. 2015. Metabolic dependencies drive species co-occurrence in diverse microbial communities. Proceedings of the National Academy of Sciences 112:6449-6454.
14. Tsoi R, Wu F, Zhang C, Bewick S, Karig D, You L. 2018. Metabolic division of labor in microbial systems. Proc Natl Acad Sci U S A 115:2526-2531.
15. Murray JL, Connell JL, Stacy A, Turner KH, Whiteley M. 2014. Mechanisms of synergy in polymicrobial infections. J Microbiol 52:188-99.
16. Hammarlund SP, Gedeon T, Carlson RP, Harcombe WR. 2021. Limitation by a shared mutualist promotes coexistence of multiple competing partners. Nat Commun 12:619.
17. Lee ED, Aurand ER, Friedman DC, Engineering Biology Research Consortium Microbiomes Roadmapping Working G. 2020. Engineering Microbiomes-Looking Ahead. ACS Synth Biol 9:3181-3183.
18. Teusink B, Molenaar D. 2017. Systems biology of lactic acid bacteria: For food and thought. Curr Opin Syst Biol 6:7-13.
19. LaSarre B, McCully AL, Lennon JT, McKinlay JB. 2017. Microbial mutualism dynamics governed by dose-dependent toxicity of cross-fed nutrients. The ISME journal 11:337-348.
20. Warnecke T, Gill RT. 2005. Organic acid toxicity, tolerance, and production in Escherichia coli biorefining applications. Microb Cell Fact 4:25.

bioRxiv preprint doi: https://doi.org/10.1101/2022.01.19.477024; this version posted January 21, 2022. The copyright holder for this preprint (which was not certified by peer review) is the author/funder, who has granted bioRxiv a license to display the preprint in perpetuity. It is made available under aCC-BY-NC-ND 4.0 International license.

21. Zengler K, Hofmockel K, Baliga NS, Behie SW, Bernstein HC, Brown JB, Dinneny JR, Floge SA, Forry SP, Hess M, Jackson SA, Jansson C, Lindemann SR, Pett-Ridge J, Maranas C, Venturelli OS, Wallenstein MD, Shank EA, Northen TR. 2019. EcoFABs: advancing microbiome science through standardized fabricated ecosystems. Nat Methods 16:567-571.
22. Beck A, Hunt K, Bernstein HC, Carlson R. 2016. Interpreting and designing microbial communities for bioprocess applications, from components to interactions to emergent properties, p 407-432. *In* Eckert CA, Trinh CT (ed), Biotechnology for Biofuel Production and Optimization. Elsevier, Amsterdam.
23. Patel A, Carlson RP, Henson MA. 2019. In Silico Metabolic Design of Two-Strain Biofilm Systems Predicts Enhanced Biomass Production and Biochemical Synthesis. Biotechnol J doi:10.1002/biot.201800511:e1800511.
24. Khan N, Maezato Y, McClure RS, Brislawn CJ, Mobberley JM, Isern N, Chrisler WB, Markillie LM, Barney BM, Song HS, Nelson WC, Bernstein HC. 2018. Phenotypic responses to interspecies competition and commensalism in a naturally-derived microbial co-culture. Sci Rep 8:297.
25. Phelps TJ, Zeikus JG. 1984. Influence of pH on Terminal Carbon Metabolism in Anoxic Sediments from a Mildly Acidic Lake. Applied and Environmental Microbiology 48:1088-1095.
26. Amarnath K, Narla AV, Pontrelli S, Dong J, Caglar T, Taylor BR, Schwartzman J, Sauer U, Cordero OX, Hwa T. 2021. doi:10.1101/2021.06.24.449802.
27. Koziolek M, Grimm M, Becker D, Iordanov V, Zou H, Shimizu J, Wanke C, Garbacz G, Weitschies W. 2015. Investigation of pH and Temperature Profiles in the GI Tract of Fasted Human Subjects Using the Intellicap((R)) System. J Pharm Sci 104:2855-63.
28. Futter MN, Valinia S, Lofgren S, Kohler SJ, Folster J. 2014. Long-term trends in water chemistry of acid-sensitive Swedish lakes show slow recovery from historic acidification. Ambio 43 Suppl 1:77-90.
29. Cai WJ, Huang WJ, Luther GW, 3rd, Pierrot D, Li M, Testa J, Xue M, Joesoef A, Mann R, Brodeur J, Xu YY, Chen B, Hussain N, Waldbusser GG, Cornwell J, Kemp WM. 2017. Redox reactions and weak buffering capacity lead to acidification in the Chesapeake Bay. Nat Commun 8:369.
30. Kremleva TA, Moiseenko TI. 2017. Evaluation of the pH buffer capacity of natural lake waters in western Siberia: Criteria of resistance to acidification. Geochemistry International 55:559-568.
31. Hummel JP, Straumfjord JV, Ellison G. 1958. Buffer Capacities of Human Blood and Plasma. Clinical Chemistry 4:452-461.
32. Salaün F, Mietton B, Gaucheron F. 2005. Buffering capacity of dairy products. International Dairy Journal 15:95-109.
33. Mennah-Govela YA, Bornhorst GM. 2020. Food buffering capacity: quantification methods and its importance in digestion and health. Food Funct doi:10.1039/d0fo02415e.
34. Little AE, Robinson CJ, Peterson SB, Raffa KF, Handelsman J. 2008. Rules of engagement: interspecies interactions that regulate microbial communities. Annu Rev Microbiol 62:375-401.
35. Zuniga C, Zaramela L, Zengler K. 2017. Elucidation of complexity and prediction of interactions in microbial communities. Microb Biotechnol 10:1500-1522.
36. Fredrickson JK. 2015. Ecological communities by design. Science 348:1425-1427.
37. Bernstein HC, Carlson RP. 2014. Design, Construction, and Characterization Methodologies for Synthetic Microbial Consortia, p 49-68. *In* Sun L, Shou W (ed), Engineering and Analyzing Multicellular Systems: Methods and Protocols. Springer New York, New York, NY.
38. Bernstein HC. 2019. Reconciling Ecological and Engineering Design Principles for Building Microbiomes. mSystems 4.
39. Brenner K, You L, Arnold FH. 2008. Engineering microbial consortia: a new frontier in synthetic biology. Trends in Biotechnology 26:483-489.

bioRxiv preprint doi: https://doi.org/10.1101/2022.01.19.477024; this version posted January 21, 2022. The copyright holder for this preprint (which was not certified by peer review) is the author/funder, who has granted bioRxiv a license to display the preprint in perpetuity. It is made available under aCC-BY-NC-ND 4.0 International license.

654 40. Park H, Patel A, Hunt KA, Henson MA, Carlson RP. 2020. Artificial consortium demonstrates
655 emergent properties of enhanced cellulosic-sugar degradation and biofuel synthesis. NPJ
656 Biofilms Microbiomes 6:59.
657 41. Repaske DR, Adler J. 1981. Change in intracellular pH of Escherichia coli mediates the
658 chemotactic response to certain attractants and repellents. Journal of Bacteriology 145:1196-
659 1208.
660 42. Han K, Levenspiel O. 1988. Extended monod kinetics for substrate, product, and cell inhibition.
661 Biotechnol Bioeng 32:430-47.
662 43. Schepens D, Beck AE, Heys JJ, Gedeon T, Carlson RP. 2017. The Benefits of Resource Partitioning
663 and Division of Labor in Microbial Consortia., p 137-148. *In* P. Amar FK, V. Norris (ed), Advances
664 in Systems and Synthetic Biology EDP Sciences Publishing.
665 44. Bernstein HC, Paulson SD, Carlson RP. 2012. Synthetic Escherichia coli consortia engineered for
666 syntrophy demonstrate enhanced biomass productivity. J Biotechnol 157:159-66.
667 45. Folsom JP, Carlson RP. 2015. Physiological, biomass elemental composition and proteomic
668 analyses of Escherichia coli ammonium-limited chemostat growth, and comparison with iron-
669 and glucose-limited chemostat growth. Microbiology 161:1659-70.
670 46. Causey TB, Zhou S, Shanmugam KT, Ingram LO. 2003. Engineering the metabolism of Escherichia
671 coli W3110 for the conversion of sugar to redox-neutral and oxidized products: homoacetate
672 production. Proc Natl Acad Sci U S A 100:825-32.
673 47. Boecker S, Zahoor A, Schramm T, Link H, Klamt S. 2019. Broadening the Scope of Enforced ATP
674 Wasting as a Tool for Metabolic Engineering in Escherichia coli. Biotechnol J 14:e1800438.
675 48. Portnoy VA, Scott DA, Lewis NE, Tarasova Y, Osterman AL, Palsson BO. 2010. Deletion of genes
676 encoding cytochrome oxidases and quinol monooxygenase blocks the aerobic-anaerobic shift in
677 Escherichia coli K-12 MG1655. Appl Environ Microbiol 76:6529-40.
678 49. Carlson RP. 2007. Metabolic systems cost-benefit analysis for interpreting network structure and
679 regulation. Bioinformatics 23:1258-1264.
680 50. Carlson RP. 2009. Decomposition of complex microbial behaviors into resource-based stress
681 responses. Bioinformatics 25:90-97.
682 51. McGill SL, Yung Y, Hunt KA, Henson MA, Hanley L, Carlson RP. 2021. Pseudomonas aeruginosa
683 reverse diauxie is a multidimensional, optimized, resource utilization strategy. Scientific Reports
684 11.
685 52. Neidhardt FC, Ingraham JL, Schaechter M. 1990. Physiology of the Bacterial Cell: A Molecular
686 Approach. Sinauer Associates Inc, Sunderland, Mass.
687 53. Patel A, Carlson RP, Henson MA. 2021. In silico analysis of synthetic multispecies biofilms for
688 cellobiose-to-isobutanol conversion reveals design principles for stable and productive
689 communities. Biochemical Engineering Journal 172.
690 54. Pacheco AR, Moel M, Segre D. 2019. Costless metabolic secretions as drivers of interspecies
691 interactions in microbial ecosystems. Nat Commun 10:103.
692 55. Pfeiffer T, Bonhoeffer S. 2004. Evolution of cross-feeding in microbial populations. Am Nat
693 163:E126-35.
694 56. Law R. 1979. Optimal Life Histories under Age-Specific Predation. American Naturalist 114:399-
695 417.
696 57. Sterner RW, Elser JJ. 2002. Ecological stoichiometry: The biology of elements from molecules to
697 the biosphere. Princeton University Press, Princeton, NJ.
698 58. Dourado H, Maurino VG, Lercher MJ. 2017. Enzymes And Substrates Are Balanced At Minimal
699 Combined Mass Concentration In Vivo. bioRxiv doi:10.1101/128009.
700 59. Schepens D, Carlson RP, Heys J, Beck AE, Gedeon T. 2019. Role of resource allocation and
701 transport in emergence of cross-feeding in microbial consortia. J Theor Biol 467:150-163.

bioRxiv preprint doi: https://doi.org/10.1101/2022.01.19.477024; this version posted January 21, 2022. The copyright holder for this preprint (which was not certified by peer review) is the author/funder, who has granted bioRxiv a license to display the preprint in perpetuity. It is made available under aCC-BY-NC-ND 4.0 International license.

60. MacLean RC, Gudelj I. 2006. Resource competition and social conflict in experimental populations of yeast. Nature 441:498-501.
61. de Mazancourt C, Schwartz MW. 2010. A resource ratio theory of cooperation. Ecology Letters 13:349-359.
62. Ausubel F, Brent R, Kingston R, Moore D, Seidman JG, Smith JA, Struhl K (ed). 1992. Short Protocols in Molecular Biology. Greene Publishing Associates and John Wiley & Sons, New York.
63. Herigstad B, Hamilton M, Heersink J. 2001. How to optimize the drop plate method for enumerating bacteria. Journal of Microbiological Methods 44:121-129.
64. Folsom JP, Parker AE, Carlson RP. 2014. Physiological and proteomic analysis of Escherichia coli iron-limited chemostat growth. J Bacteriol 196:2748-61.
65. Lendenmann U, Egli T. 1998. Kinetic models for the growth ofEscherichia coli with mixtures of sugars under carbon-limited conditions. Biotechnology and Bioengineering 59:99-107.
66. Klamt S, von Kamp A. 2011. An application programming interface for CellNetAnalyzer. Biosystems 105:162-8.

FIGURE LEGENDS

Figure 1. Inhibition of wildtype *E. coli* cultures as a function of organic acids, pH, and osmotic pressure. (A) and **(B)** *E. coli* specific growth rate in conventional M9 medium as a function of acetic acid and lactic acid concentration when the organic acids were the sole substrates. (A) Abscissa plots the total concentration of the metabolite (protonated (HA) and unprotonated (A^-)). (B) Abscissa plots only the protonated metabolite (HA) concentration. Colored lines represent the specific growth rate predicted with best-fit models. Best fit equations and parameters listed in Table 1. **(C)** and **(D)** *E. coli* specific growth rate in conventional M9 medium as a function of acetic acid and lactic acid concentration when 56 mM glucose was added in addition to the organic acid. (A) Abscissa plots the total concentration of the metabolite (protonated (HA) and unprotonated (A^-)). (B) Abscissa plots only the protonated metabolite (HA) concentration. Colored lines represent the specific growth rate predicted with best-fit models. Best fit equations and parameters are listed in Table 1. **(E)** Specific growth rate of *E. coli cultures* as a function of medium pH. Cultures grown in conventional M9 medium with 56 mM glucose as the sole carbon source (no added organic acids). **(F)** Effect of osmotic pressure on specific growth rate of *E. coli* cultures. Growth was tested at 1X, 1.5X, 2X, and 2.5X the concentration of conventional M9 medium components (converted to concentration of dissolved solutes with Visual MINTEQ 3.1). Each point represents the average of at least three biological replicates with error bars representing standard deviation.

bioRxiv preprint doi: https://doi.org/10.1101/2022.01.19.477024; this version posted January 21, 2022. The copyright holder for this preprint (which was not certified by peer review) is the author/funder, who has granted bioRxiv a license to display the preprint in perpetuity. It is made available under aCC-BY-NC-ND 4.0 International license.

Figure 2. Schematic representations of the central metabolism of the five *E. coli* phenotypic guilds: generalist (Wild type), producer secreting acetic acid (ProdA), consumer catabolizing acetic acid (ConsA), producer secreting lactic acid (ProdL), and consumer catabolizing lactic acid (ConsL). Metabolite exchanges necessitate costs which are translated into fitness considerations for the five guilds including catabolic efficiency of relevant substrate, ATP opportunity costs for a guild phenotype, and central metabolism proteome investment costs. Numbers in figures refer to enzyme catalyzed reactions, see supplementary material for key. AA = amino acids, Cmol = carbon mole, mol = mole.

Figure 3. Wild type culture (generalist guild) properties as a function of initial medium pH. A) Biomass accumulation with time as a function of initial medium pH. **B)** Specific growth rate as a function of initial medium pH. **C)** pH as a function of time for cultures starting at different initial pH values. **D)** Acetic acid concentration as a function of time for cultures starting at different initial pH values. Error bars represent the standard deviation of three biological samples.

Figure 4. Acetic acid exchanging (AAE) consortium as a function of initial pH. **A)** Consortium biomass concentration with time for four different initial medium pH values. **B)** Consortium specific growth rate as a function of initial medium pH. **C)** Medium pH with time as a function of initial medium pH. **D)** Comparison of AAE consortium to acetic acid producer (ProdA) monoculture as a function of initial pH. **E)** Acetic acid concentration with time as a function of initial medium pH. **F)** Cell fraction of ProdA guild to ConsA guild with time as a function of initial medium pH. Data is mean of three biological replicates which error bars representing standard deviation.

Figure 5. Lactic acid exchanging (LAE) consortium as a function of initial pH. **A)** Consortium biomass concentration with time for four different initial pH values. Note the upper time axis for the culture with an initial pH of 7.5. **B)** Consortium specific growth rate as a function of initial medium pH. **C)** pH with time as a function of initial medium pH. **D)** Comparison of LAE consortium to lactic acid producer (ProdL) monoculture as a function of initial pH. **E)** Lactic acid concentration with time as a function of initial medium pH. **F)** Cell fraction of ProdL guild to ConsL guild with time as a function of initial medium pH. Data is mean of three biological replicates which error bars representing standard deviation.

bioRxiv preprint doi: https://doi.org/10.1101/2022.01.19.477024; this version posted January 21, 2022. The copyright holder for this preprint (which was not certified by peer review) is the author/funder, who has granted bioRxiv a license to display the preprint in perpetuity. It is made available under aCC-BY-NC-ND 4.0 International license.

Figure 6. Lactic acid exchanging (LAE) consortium as a function of different initial guild ratios. **A)** Consortium biomass concentration with time for different initial guild cell ratios. **B)** Medium pH with time as a function of different initial guild cell ratios. **C)** Lactic acid concentration with time for different initial guild cell ratios. **D)** Cell fraction of ProdL guild to ConsL guild with time as a function of initial cellular ratios. **F)** Acetic acid concentration with time as a function of initial guild ratios.

Figure 7. Summary of fitness metrics for organic acid exchanging consortia compared to producer monocultures and wild type monocultures. A) Total glucose consumed during batch growth. **B)** Biomass (g cdw) produced per mole H^+ accumulated in medium. **C)** Final biomass concentration (g cdw L^{-1}) at stationary phase. **D)** Biomass yield on glucose (g cdw (g glucose)$^{-1}$). Each circle represents one biological sample. Mean values for each condition denoted with line. cdw = cell dry weight.

Figure 8. Fitness metrics for lactic acid exchanging (LAE) consortium compared to wild type generalist in highly buffered M9 medium. A) Total glucose consumed during batch growth. **B)** Biomass (g cdw) produced per mole H^+ accumulated in medium. **C)** Final biomass concentration (g cdw L^{-1}) at stationary phase. **D)** Biomass yield on glucose (g cdw (g glucose)$^{-1}$). Each circle represents one biological sample. Mean value for each condition denoted with line. cdw = cell dry weight.

bioRxiv preprint doi: https://doi.org/10.1101/2022.01.19.477024; this version posted January 21, 2022. The copyright holder for this preprint (which was not certified by peer review) is the author/funder, who has granted bioRxiv a license to display the preprint in perpetuity. It is made available under aCC-BY-NC-ND 4.0 International license.

781 **TABLES**

782 **Table 1.** Best-fit expressions and parameters used to model organic acid growth and inhibition kinetics for
783 wild type *E. coli*.
784

Condition	Best-fit Expression	Parameters
Acetic acid as sole substrate	$\mu = \mu_C \left(\frac{A}{K_G+A}\right) e^{-\frac{A}{K_I}}$, where μ is growth rate (h^{-1}) and A is concentration of protonated acetate (mM)	μ_C = 0.470 h^{-1}, K_G = 0.0948 mM, and K_I = 0.669 mM
Lactic acid as sole substrate	$\mu = \mu_C \left(\frac{L}{K_G+L}\right) e^{-\frac{L}{K_I}}$, where μ is growth rate (h^{-1}) and L is concentration of protonated lactate (mM)	μ_C = 0.485 h^{-1}, K_G = 0.0034 mM, and K_I = 0.339 mM
Acetic acid with glucose	$\mu = \mu_C \left(\frac{G}{K_G+G}\right) e^{-KA}$, where μ is growth rate (h^{-1}), G is concentration of glucose (set to 56 mM), and A is concentration of protonated acetate (mM)	μ_C = 0.974 h^{-1}, K_G = 27.29 mM, and K = 1.365 mM
Lactic acid with glucose	$\mu = \mu_{max}\left[\left(\frac{G}{K_G+G}\right) + \left(\frac{L}{K_L+L}\right)\right] e^{-\alpha L}$, where μ is growth rate (h^{-1}), G is concentration of glucose (set to 56 mM), and L is concentration of protonated lactate (mM)	μ_{max} = 0.767 h^{-1}, K_G = 7.051 mM, K_L = 0.115 mM, and α = 4.6 $mmol^{-1}$
pH	$\mu = \mu_{max}\left(1 - \frac{H}{H^*}\right)$, where μ is growth rate (h^{-1}), and H is concentration of protons (M)	μ_{max} = 0.665 h^{-1}, and H^* = $10^{-4.4}$ M (critical threshold above which growth is not possible)

785

786
787

bioRxiv preprint doi: https://doi.org/10.1101/2022.01.19.477024; this version posted January 21, 2022. The copyright holder for this preprint (which was not certified by peer review) is the author/funder, who has granted bioRxiv a license to display the preprint in perpetuity. It is made available under aCC-BY-NC-ND 4.0 International license.

Table 2. Physiological properties of *E. coli* generalist and producer/consumer guilds in monoculture. Measurements were obtained from growth on conventional M9 medium containing 4 g L^{-1} glucose (for generalist and producer specialists) or 1 g L^{-1} sodium acetate or 2.8 g L^{-1} sodium lactate for consumer specialists.

	Generalist (WT)	**Acetate Producer** (ProdA)	**Lactate Producer** (ProdL)	**Consumer** (ConsA/ConsL)
Carbon source	Glucose (*n*=4)	Glucose (*n*=3)	Glucose (*n*=9)	Acetic acid (*n*=2) / Lactic acid (*n*=9)
Maximum growth rate	0.65 h^{-1} ± 0.01	0.54 h^{-1} ± 0.007	0.24 h^{-1} ± 0.003	0.14 h^{-1} ± 0.003 / 0.41 h^{-1} ± 0.01
Biomass yield	0.43 g biomass per g glucose ± 0.02	0.20 g biomass per g glucose ± 0.01	0.05 g biomass per g glucose ± 0.001	0.24 g biomass per g acetic acid ± 0.005 / 0.48 g biomass per g lactic acid ± 0.01
Organic byproduct yield	0.11 g acetic acid per g glucose ± 0.01	0.34 g acetic acid per g glucose ± 0.004	0.86 g lactic acid per g glucose ± 0.01	NA

Notes: the consumer guild is capable of growth on glucose but at a very low rate (0.016 h^{-1}). The lactic acid producer accumulates minor amounts of acetic acid (< 0.06 g/L) and succinic acid (< 0.12 g/L) in addition to lactic acid during stationary phase, which aligns with results reported in (48).

bioRxiv preprint doi: https://doi.org/10.1101/2022.01.19.477024; this version posted January 21, 2022. The copyright holder for this preprint (which was not certified by peer review) is the author/funder, who has granted bioRxiv a license to display the preprint in perpetuity. It is made available under aCC-BY-NC-ND 4.0 International license.

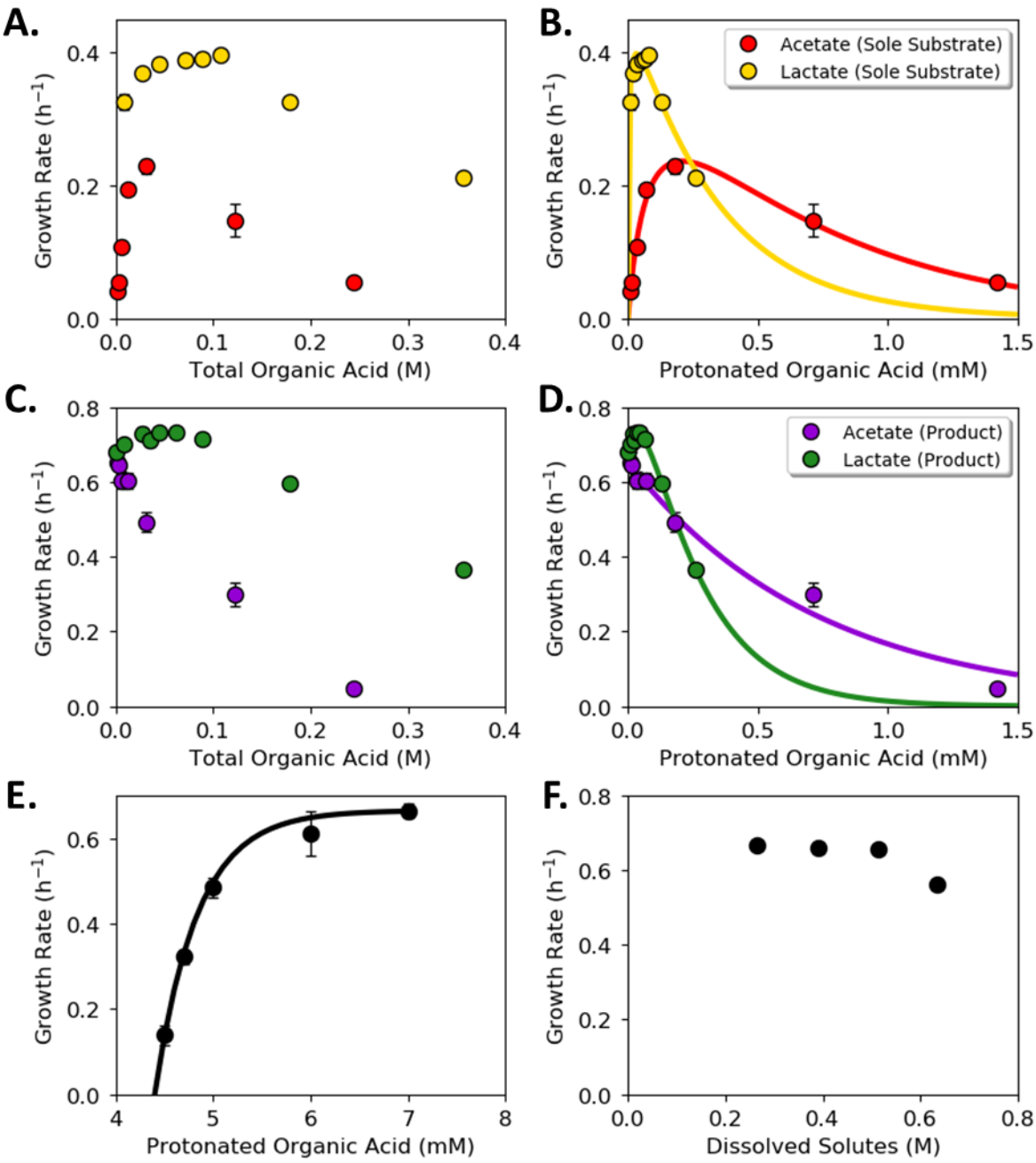

800

801 Figure 1.

802

bioRxiv preprint doi: https://doi.org/10.1101/2022.01.19.477024; this version posted January 21, 2022. The copyright holder for this preprint (which was not certified by peer review) is the author/funder, who has granted bioRxiv a license to display the preprint in perpetuity. It is made available under aCC-BY-NC-ND 4.0 International license.

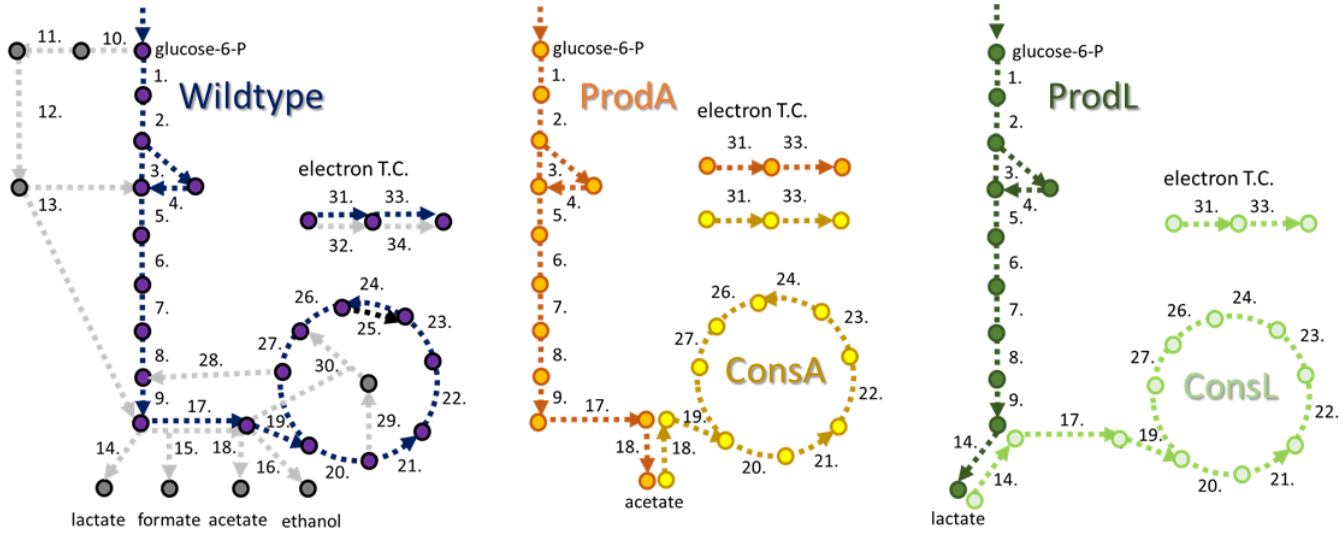

	WT	ProdA	ConsA	ProdL	ConsL
Catabolic efficiency (ATP (mol substrate)$^{-1}$)	26	4	6	2	12
Catabolic efficiency (Cmol substrate (ATP)$^{-1}$)	0.23	1.5	0.29	3	0.25
Opportunity cost (ATP (mol glucose)$^{-1}$)		22		24	
Total proteome investment (Amino Acids (AA))	101,548	63,424	49,047	13,662	89,646
Total proteome investment (ATP equivalents)	2,597,136	528,533	1,409,397	227,700	2,390,560
Normalized proteome investment (AA (ATP)$^{-1}$)	3,906	15,856	8,175	6,831	7,471
Normalized proteome investment (ATP equiv. (ATP)$^{-1}$)	99,890	132,133	234,899	113,850	199,213

Figure 2.

bioRxiv preprint doi: https://doi.org/10.1101/2022.01.19.477024; this version posted January 21, 2022. The copyright holder for this preprint (which was not certified by peer review) is the author/funder, who has granted bioRxiv a license to display the preprint in perpetuity. It is made available under aCC-BY-NC-ND 4.0 International license.

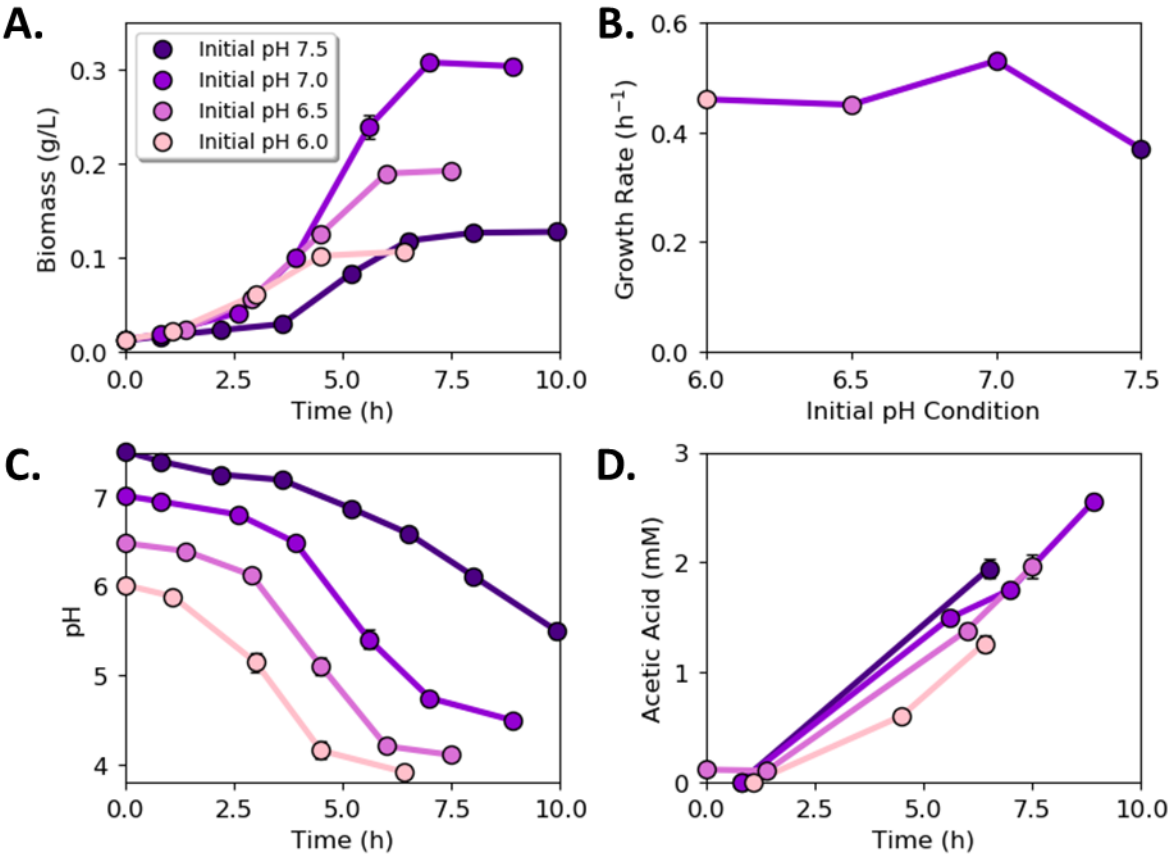

807

808

809 Figure 3.

810

811

bioRxiv preprint doi: https://doi.org/10.1101/2022.01.19.477024; this version posted January 21, 2022. The copyright holder for this preprint (which was not certified by peer review) is the author/funder, who has granted bioRxiv a license to display the preprint in perpetuity. It is made available under aCC-BY-NC-ND 4.0 International license.

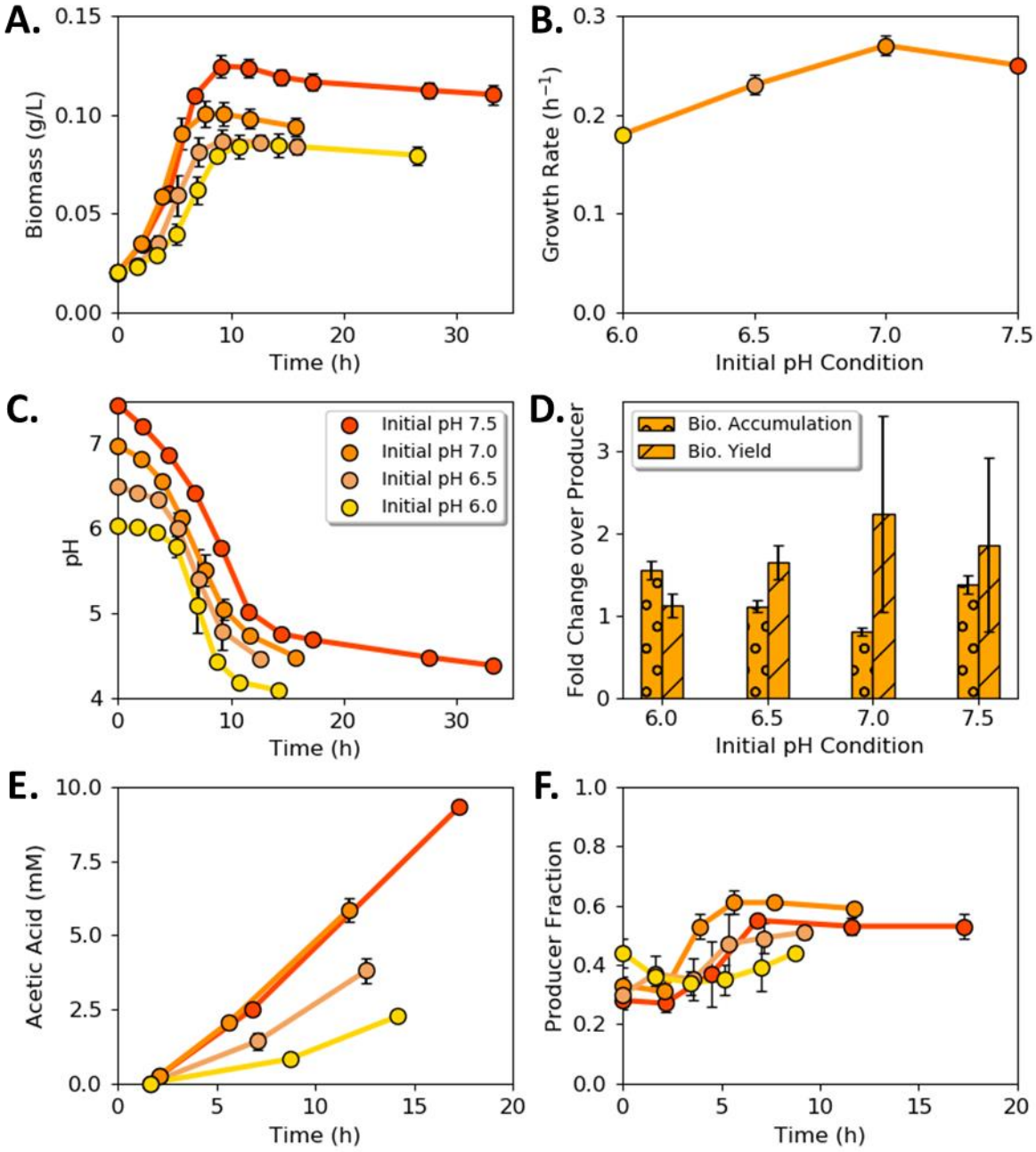

Figure 4.

bioRxiv preprint doi: https://doi.org/10.1101/2022.01.19.477024; this version posted January 21, 2022. The copyright holder for this preprint (which was not certified by peer review) is the author/funder, who has granted bioRxiv a license to display the preprint in perpetuity. It is made available under aCC-BY-NC-ND 4.0 International license.

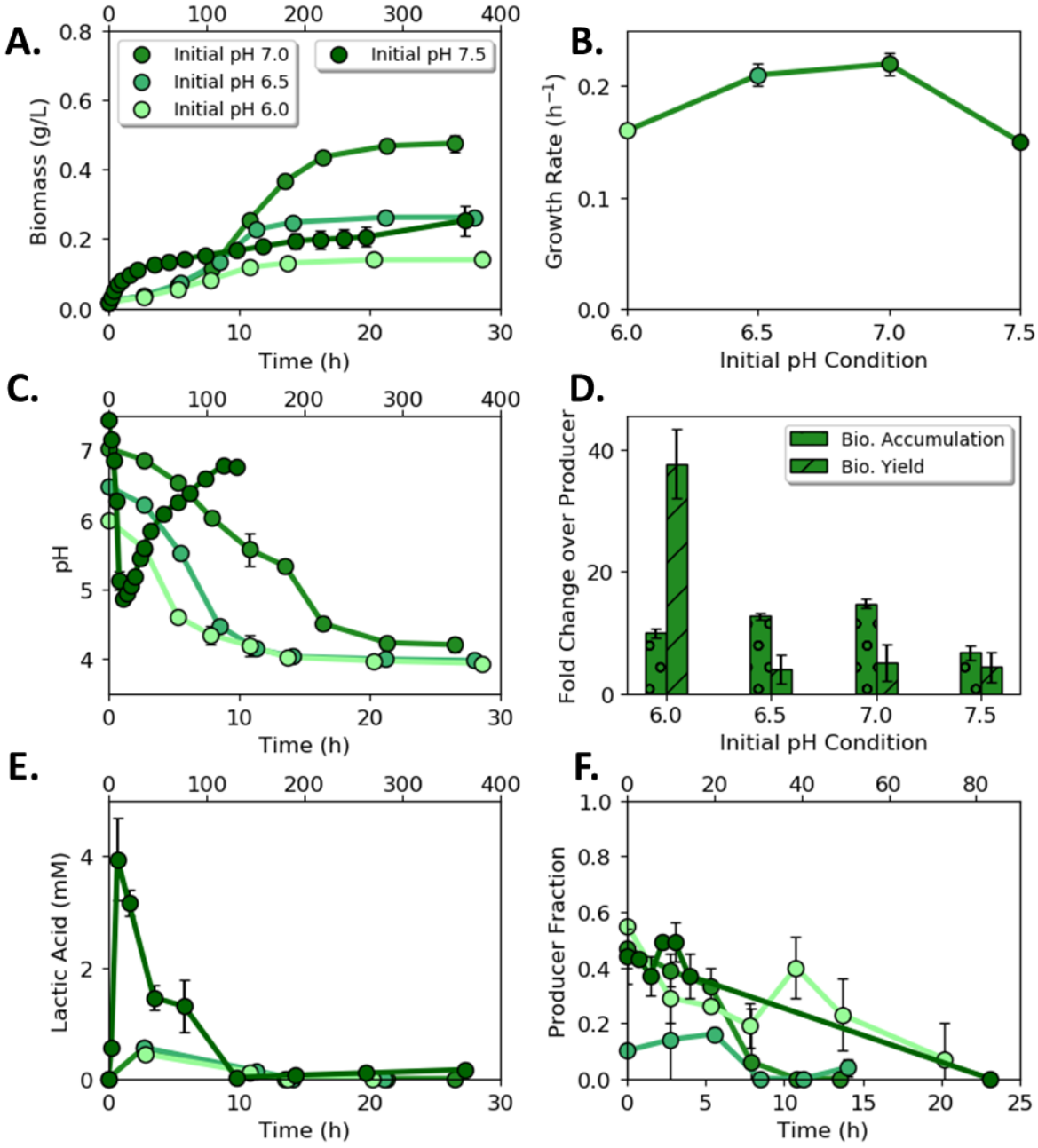

817

818

819 Figure 5.

820

821

bioRxiv preprint doi: https://doi.org/10.1101/2022.01.19.477024; this version posted January 21, 2022. The copyright holder for this preprint (which was not certified by peer review) is the author/funder, who has granted bioRxiv a license to display the preprint in perpetuity. It is made available under aCC-BY-NC-ND 4.0 International license.

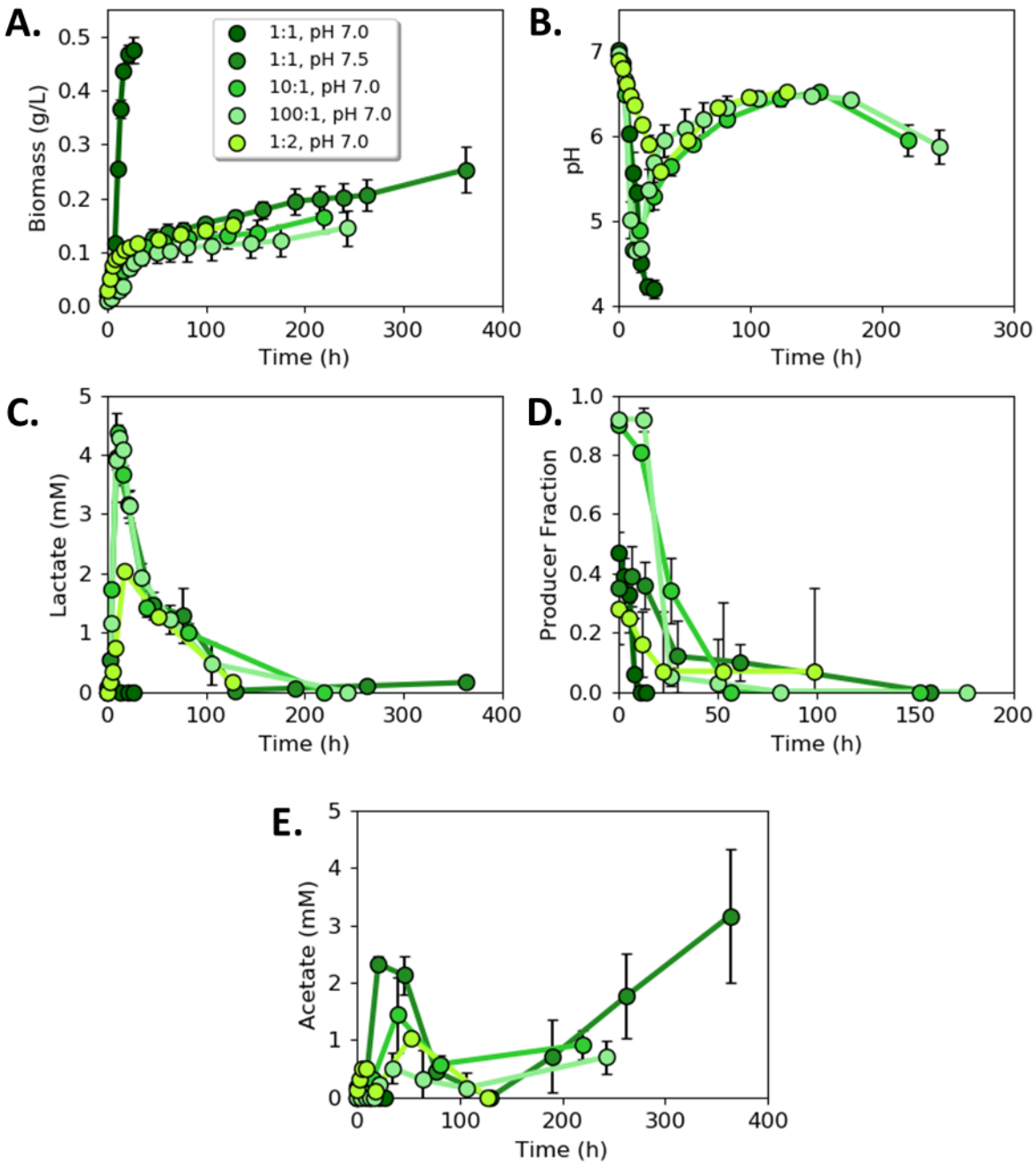

822

823

824 Figure 6.

825

826

bioRxiv preprint doi: https://doi.org/10.1101/2022.01.19.477024; this version posted January 21, 2022. The copyright holder for this preprint (which was not certified by peer review) is the author/funder, who has granted bioRxiv a license to display the preprint in perpetuity. It is made available under aCC-BY-NC-ND 4.0 International license.

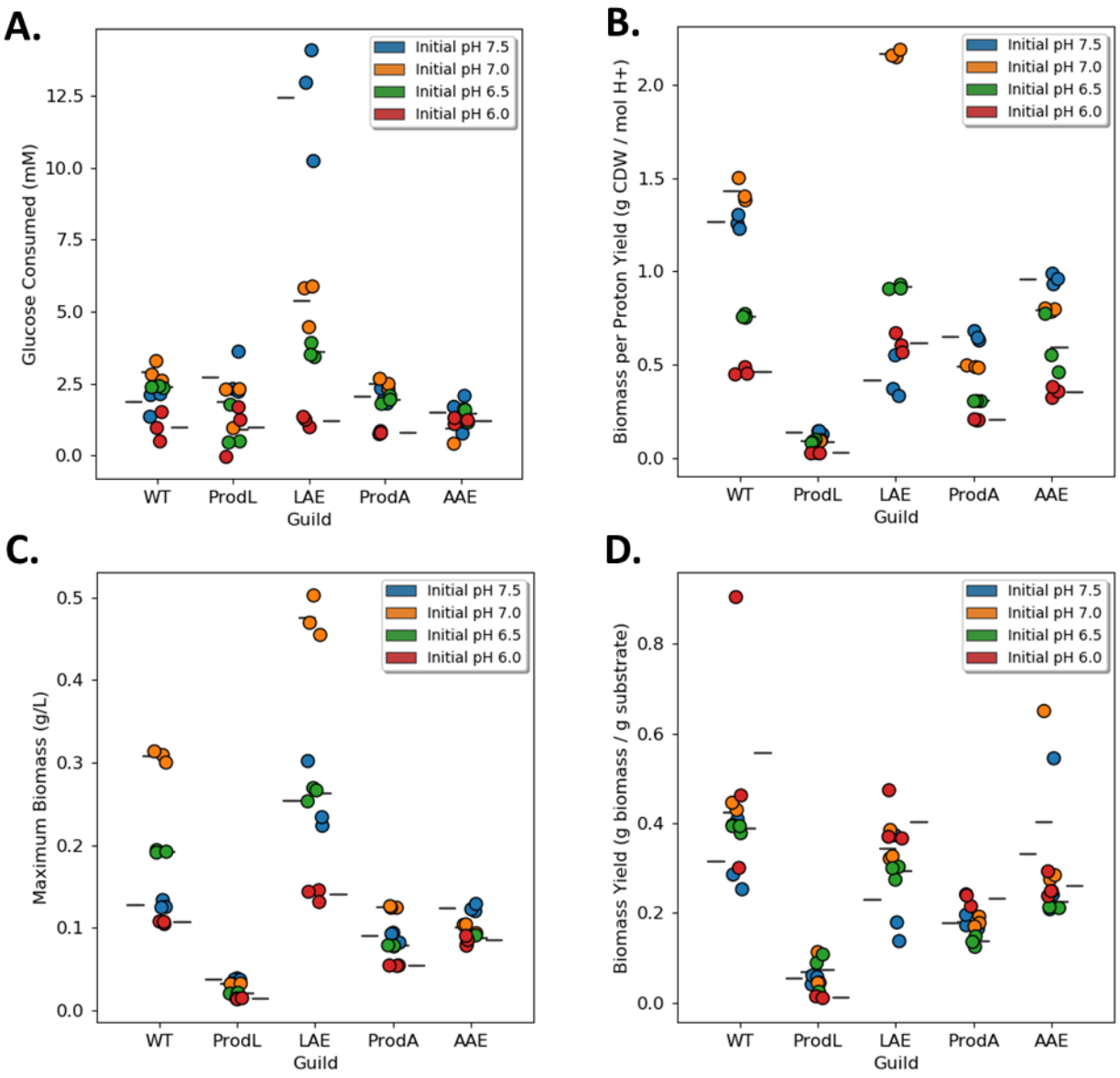

827

828

829 Figure 7.

830

831

bioRxiv preprint doi: https://doi.org/10.1101/2022.01.19.477024; this version posted January 21, 2022. The copyright holder for this preprint (which was not certified by peer review) is the author/funder, who has granted bioRxiv a license to display the preprint in perpetuity. It is made available under aCC-BY-NC-ND 4.0 International license.

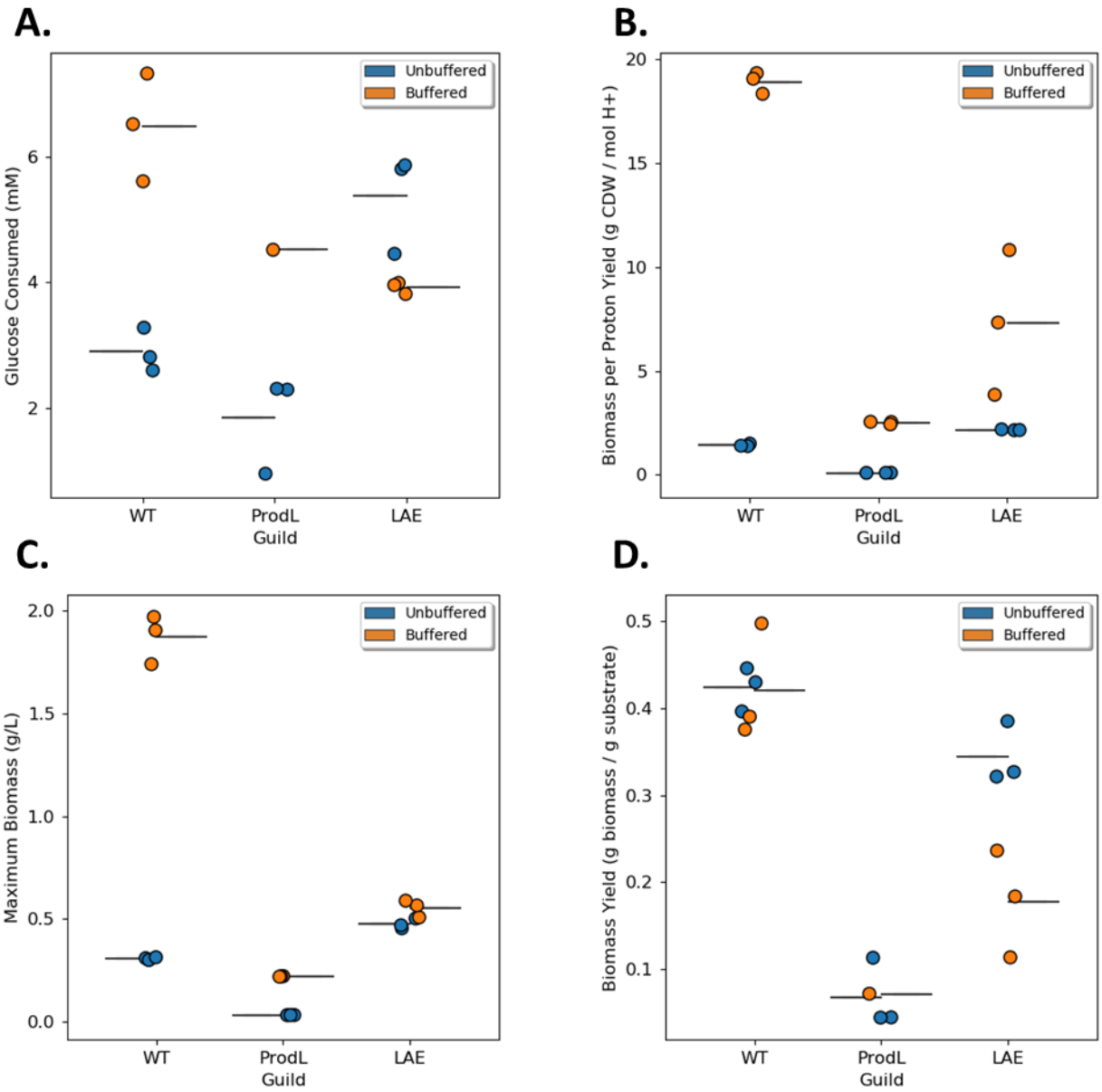

832

833

834 Figure 8.